ANALOGUE TECHNIQUE FOR MAPPING POISSONIAN FIELDS

ANALOGUE TECHNIQUE FOR MAPPING POISSONIAN FIELDS

by

Paul Victor Birke, B.A.Sc.

A Thesis

Submitted to the Faculty of Graduate Studies

in Partial Fulfillment of the Requirements

for the Degree

Master of Engineering

McMaster University

May, 1970

MASTER OF ENGINEERING (1970) McMASTER UNIVERSITY
(Electrical Engineering) Hamilton, Ontario

TITLE: Analogue Technique for Mapping Poissonian Fields

AUTHOR: Paul Victor Birke, B.A.Sc. (University of Toronto)

SUPERVISOR: Professor R. Kitai

NUMBER OF PAGES: (x); 96:

SCOPE AND CONTENTS: A review of the conducting paper analogue for plotting two-dimensional electric and magnetic fields is given. An improved capacitively-coupled conducting paper analogue is described that will map either single or multiple, uniformly-distributed-source Poissonian fields. A new map construction technique is detailed that uses a thin tape dielectric and silver-painted source electrodes. Equipotentials on the conducting paper surface correspond to lines of constant magnetic vector potential or flux lines. Differential voltages are analogous to flux density. The equipotential distribution is plotted using a null technique with a unique point on the map surface held at virtual ground potential. The time-varying equations governing the capacitively-coupled analogue are derived. As a result of these equations, an analogue for the skin effect phenomenon in conductors has been demonstrated.

ACKNOWLEDGEMENTS

I am indebted to Professor Reuven Kitai for his initial support of this topic and his guidance during the preparation of this thesis.

I would like to thank the Canadian Westinghouse Co.Ltd. and in particular, Mr. V. Mason and Mr. J. Harbell of the Power Transformer and Circuit Breaker Division for the financial support given to me and the project. This work was initiated in the Power Transformer and Circuit Breaker Division.

For the useful discussions with Jay Mijithia, Desmond Taylor, and Magid Dimyan, I wish to express my thanks.

Finally, to Mrs. E. Intson, my sincere appreciation for typing this thesis.

TABLE OF CONTENTS

Table of Contents Cont'd — Page

LIST OF ILLUSTRATIONS

List of Illustrations

LIST OF TABLES

LIST OF SYMBOLS

Symbol	Quantity	Unit
$A_z(x,y)$	two-dimensional magnetic vector potential	weber/metre
B	magnetic flux density	tesla
C	capacitance	farad (F)
C'	capacitance per unit area	farad/metre^2
D	electric flux density	coulomb/metre^2
E	electric field intensity	volt/metre
f	frequency	Hertz
H	magnetic field intensity	ampere/metre
I	electric current	ampere
J	electric current density	ampere/metre^2
J , Y	Bessel functions	-
j	$\sqrt{-1}$	-
K	resistance per square	ohm(Ω)
$k_o, k_1, \ldots$	constants	-
l	length	metre
R	resistance	ohm
R'	resistance per unit length	ohm/metre
r	radius	metre
T	thickness	metre
t	time	second
	or tangential	-

List of Symbols Cont'd

Symbol	Quantity	Unit
$u(\ )$	function	-
V	voltage	volt
$V(x,y)$	surface voltage distribution	volt
X_c	capacitance reactance	ohm
Z	impedance	ohm
ε_o	permittivity of free space	coulomb/ volt-metre
ε_r	relative permittivity	numeric
μ_o	permeability of free space	weber/ ampere-metre
μ_r	relative permeability	numeric
σ	electrical conductivity	mho/metre
ρ	electrical resistivity	ohm-metre
δ	constant	-
λ	variable	-
ω	angular frequency	radian/second
ϕ'	magnetic flux per unit length	weber/metre
$\theta,\phi,\alpha,\beta,\psi$	phase angle	radian
$\Delta(\ )$	increment of $(\ )$	-
∇	gradient operator	metre^{-1}
∇^2	Laplacian operator	metre^{-2}
$\nabla\cdot$	divergence operator	metre^{-1}
∇x	curl operator	metre^{-1}

CHAPTER 1

1.1 Introduction

There are many analogies in science. Analogies allow the qualitative and often quantitative analysis of a real system. Two systems are analogous if they have a common basis of interchangeable mathematics. As analogies are seldom perfect, it is usually sufficient if the equations describing the analogue system are known to approximate the real equations to within a definable but small error. Often, the equations governing the real system may have to be idealized in order to allow an analogous formulation.

An analogue justifies its use if it can simplify obtaining information about the real system; that is, if it can save time. A good analogue should have its system variables flexible. This allows the most general and efficient use of the analogue system in interpreting the real system.

The use of analogue techniques is a very useful tool in engineering research and teaching; although recently, there has been a tendency to minimize the use of experimental analogues. However, many problems or their analogue equivalents may be simulated on the modern digital computer. In fact, computer simulation has become a standard approach to

such problems. As a consequence, actual experimental setups of the real problem or its analogy tend to suffer as an engineering approach. However, there are many areas in which experimental analogues are well justified, and field mapping may be classed as one of these.

1.2 Conducting-Paper Analogues

In electrical engineering certain two-dimensional electric and magnetic field distributions can be simulated on a conducting-paper analogue. The electroconduction field in a uniformly-conductive paper sheet comprises of the current flow lines and the equipotential lines. The analogue is defined to be a direct type when the current flow lines correspond to the flux lines of the electric or magnetic field. The orthogonal analogue has the equipotentials representing flux lines. In the orthogonal analogue, conducting boundaries on the paper represent flux-impermeable surfaces or known flux lines. Non-conducting boundaries represent flux-permeable surfaces or known symmetry planes. The converse of these boundary conditions is true for the direct analogue.

Two-dimensional electric and magnetic field distributions for the stationary and quasi-stationary time case fall into three general categories. These are:

(a) field distributions which satisfy Laplace's

equation $\nabla^2\phi(x,y) = 0$.

(b) field distributions which satisfy Poisson's equation in scalar form $\nabla^2\phi(x,y) \neq 0$ or in vector form $\nabla^2\vec{\phi}(x,y) \neq 0$.

(c) field distributions which satisfy Laplace's equation in some regions and Poisson's equation (scalar or vector form) in other separate (source) regions of the field. Examples of these different field distributions are shown in Figure 1:1.

1.2.1 DC Laplacian Analogue

The dc conducting-paper (Teledeltos) analogue has been used for many years to solve Laplacian field problems.[1] The Laplacian Teledeltos mapping system provides quick solutions to extremely complicated electrode and boundary configurations with good engineering accuracy. The basic system is illustrated in Figure 1:2.

1.2.2. Multiple Pin DC Poissonian Analogue

This orthogonal system was the first proposed conducting-paper analogue to simulate the Poissonian field.[2,3,4,5] Each source region is a matrix of pins, each delivering a constant current into the conducting sheet. Constant current is obtained using large resistances in series with each feed point. The voltage drop across any

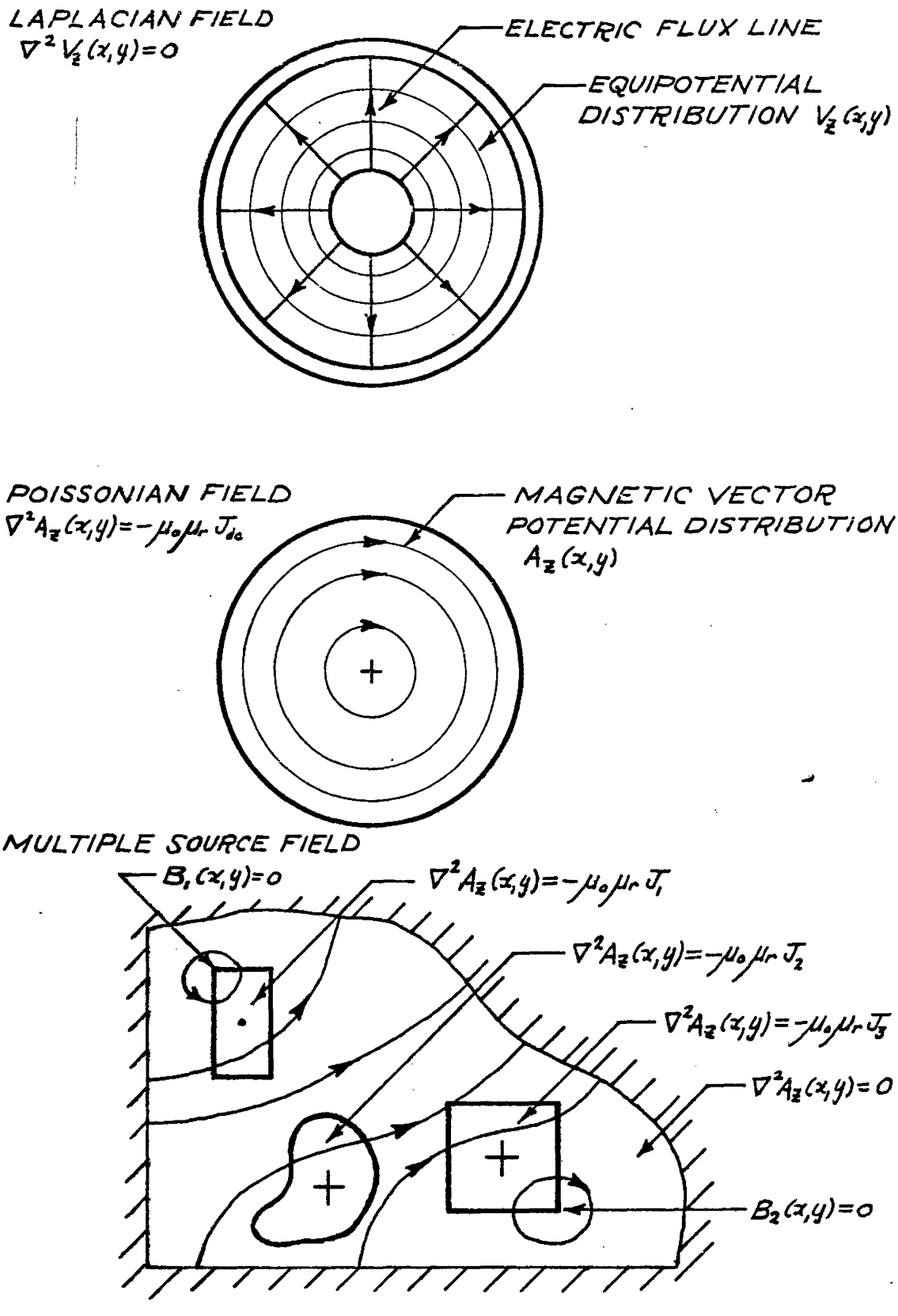

FIGURE 1.1 TWO-DIMENSIONAL FIELD DISTRIBUTIONS

REAL SYSTEM :- COAXIAL CABLE

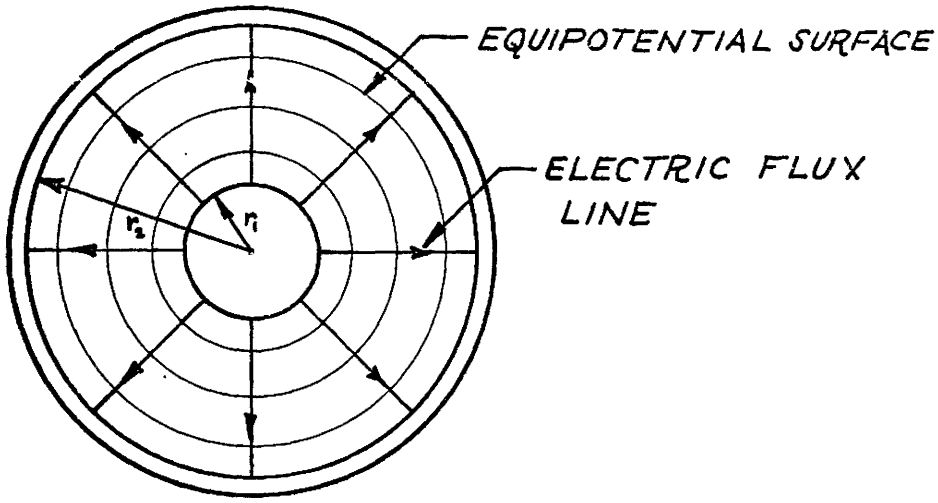

ANALOGUE SYSTEMS :- (i) ORTHOGONAL ANALOGUE

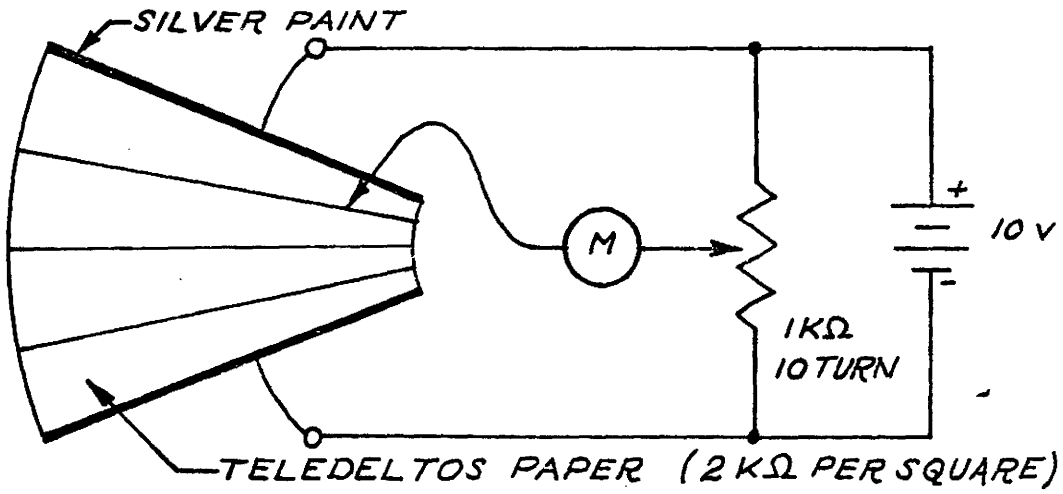

(ii) DIRECT ANALOGUE

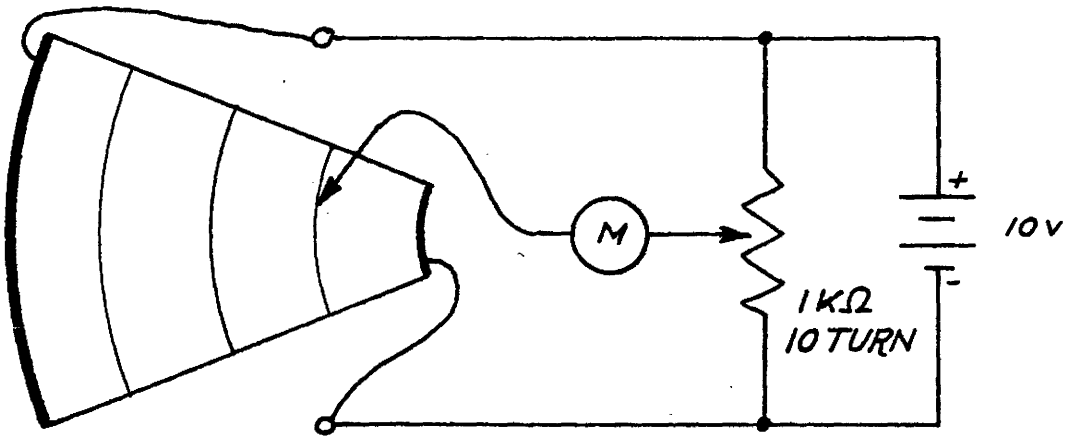

FIGURE 1.2 LAPLACIAN FIELD TELEDELTOS ANALOGUE

of these resistors is much greater than the maximum voltage difference found on the paper surface. There is a direct correspondence between the magnitude of the effective current density in each source region with that of the real field.

Although the analogue enjoys the simplicity of using dc, it has, however, some disadvantages. These are:

(a) An elaborate experimental setup is needed for accurate results, because hundreds of pins may be inserted in the conducting paper.

(b) There is the tedious procedure of actually connecting the pins and adjusting each current feed point.

The basic system is exemplified in Figure 1:3.

1.2.3 AC Capacitively-Coupled Poissonian Analogue

In 1953, the Gilbert twins, then at the University of Michigan at Ann Arbor, described an analogue system that could map two-dimensional uniformly-distributed source fields.[6] Their unique mapping system (shown in Figure 1:4) incorporates a Teledeltos resistive mapping surface and a capacitively-coupled electrode whose geometry has the same proportions as the real source. The coupling capacitor is formed using an aluminum foil electrode glued to a thin glass dielectric. When the excitation frequency is low enough, the

RECTANGULAR CONDUCTOR IN IRON SLOT

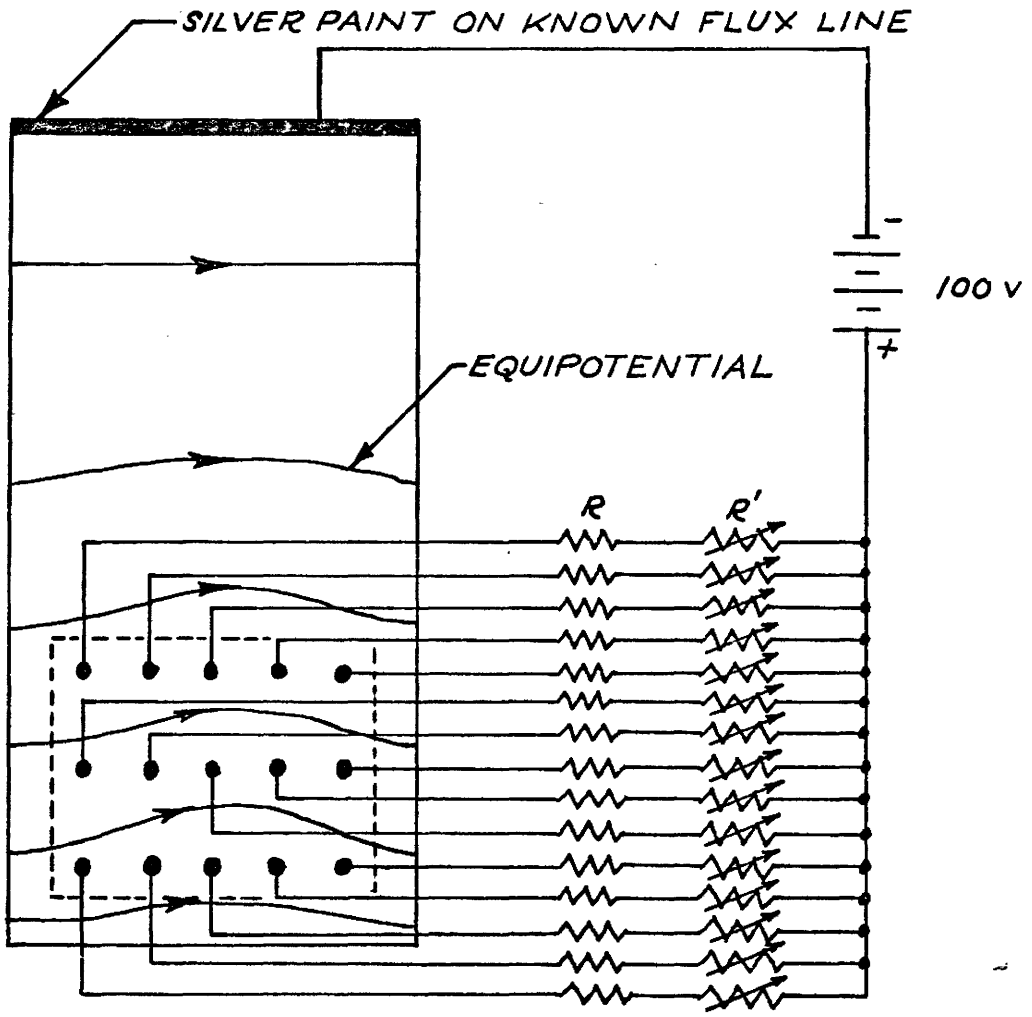

FEED POINT CONNECTION ARRANGEMENT

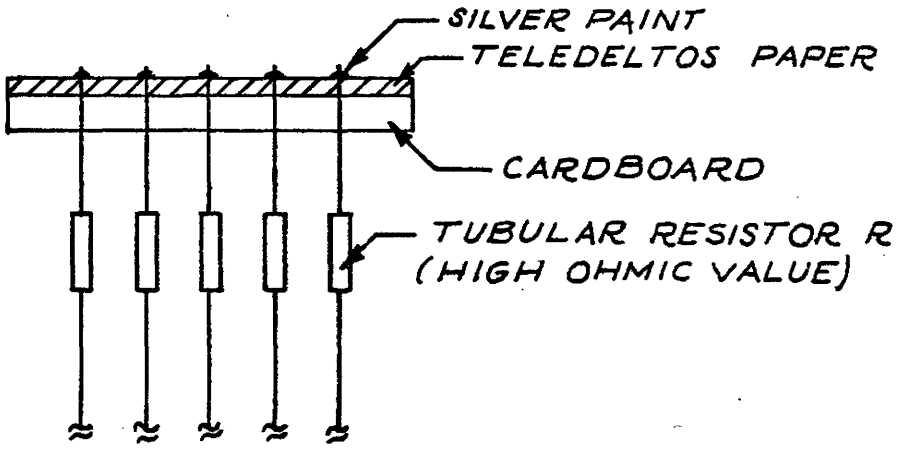

FIGURE 1.3 MULTIPLE PIN DC POISSONIAN ANALOGUE

CONDUCTOR CARRYING DC

POISSONIAN FIELD MAP
(ORTHOGONAL TYPE)

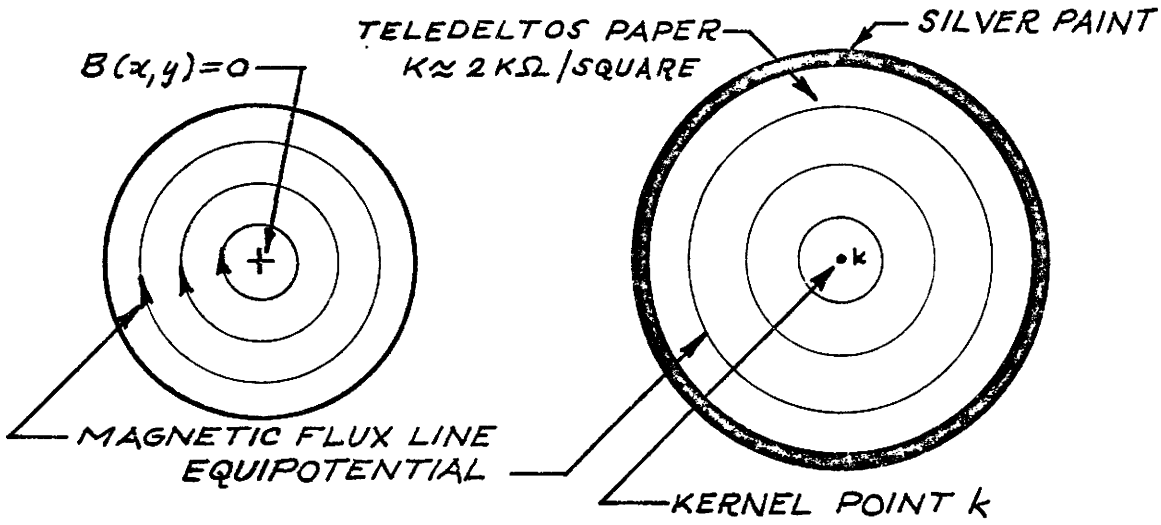

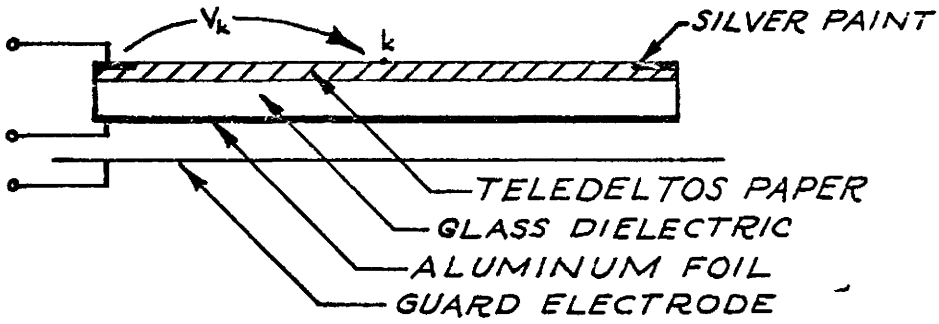

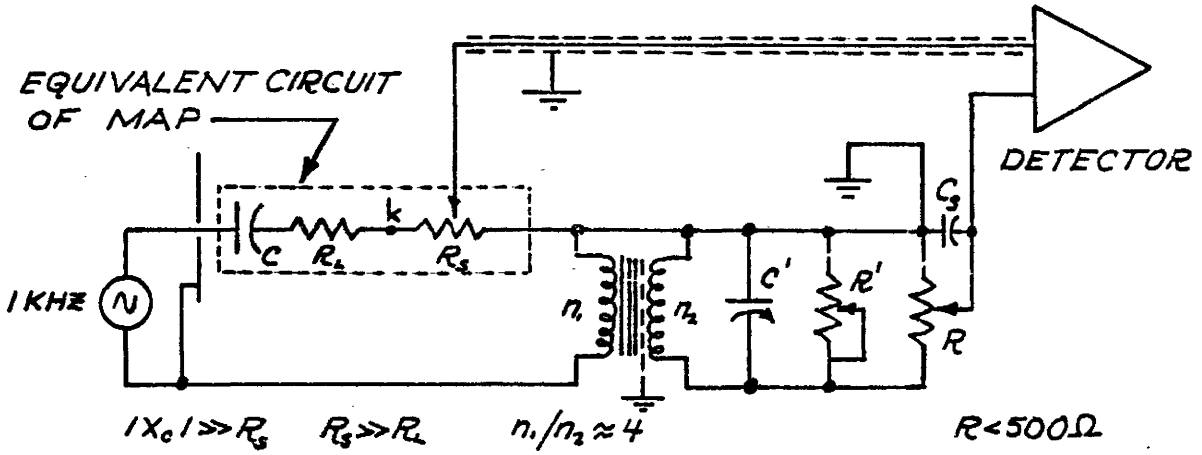

FIGURE 1.4 GILBERT POISSONIAN ANALOGUE

capacitive reactance formed between the foil electrode and the conducting paper surface is much greater than the equivalent surface resistance of the paper. Then, the capacitive displacement current density J_c is inversely proportional to the dielectric thickness T_d. The current density J_c over the source region is therefore constant if the dielectric is of uniform thickness.

The voltage distribution V(x,y) on the Teledeltos surface satisfies the Poissonian equation $\nabla^2 V(x,y) = -KJ_c \angle -90°$ where K is the resistance per square of the Teledeltos paper. This very fundamental equation can be derived with the assumption that the thickness of the conducting paper is sufficiently small to ensure that the current flowing in the plane of the paper is independent of any axial variation. An elemental section of the paper-dielectric sandwich for a capacitively-coupled region is shown in Figure 1:5.

If Kirchoff's current law is applied to the conducting-paper elemental section one has

$$J(x,t)\, T_p \Delta y + J(y,t)\, T_p \Delta x + J_c(t)\, \Delta x \Delta y =$$

$$\left(J(x,t) + \frac{\partial J(x,t)}{\partial x} \Delta x\right) T_p \Delta y + \left(J(y,t) + \frac{\partial J(y,t)}{\partial y} \Delta y\right) T_p \Delta x$$

where J represents current density in amperes/metre^2, giving

$$\frac{\partial J(x,t)}{\partial x} + \frac{\partial J(y,t)}{\partial y} = \frac{J_c(t)}{T_p} \qquad \text{.....1.1}$$

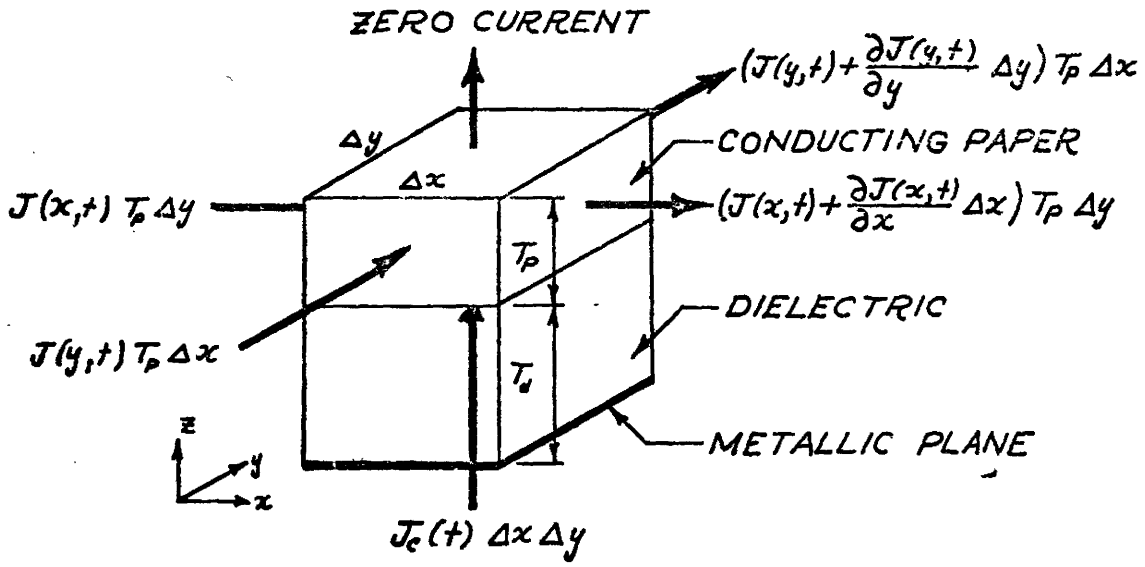

FIGURE 1.5 CURRENTS IN AN ELEMENTAL PAPER SECTION

From Ohm's law it is seen that, if E represents electric field strength in volts/meter,

$$E(x,t) = -\rho J(x,t) \quad \text{or} \quad \frac{\partial V(x,y,t)}{\partial x} = -\rho J(x,t) \quad .....1.2$$

$$E(y,t) = -\rho J(y,t) \quad \text{or} \quad \frac{\partial V(x,y,t)}{\partial y} = -\rho J(y,t) \quad .....1.3$$

where ρ is the resistivity of the conducting paper in ohm-metres. On rearrangement of equations 1.2 and 1.3 and substitution into equation 1.1 one has

$$\frac{\partial}{\partial x}\left(\frac{-1}{\rho}\frac{\partial V(x,y,t)}{\partial x}\right) + \frac{\partial}{\partial y}\left(\frac{-1}{\rho}\frac{\partial V(x,y,t)}{\partial y}\right) = \frac{J_c(t)}{T_p} \quad .....1.4$$

The resistivity of the conducting paper is related to its resistance per square and thickness by

$$\rho = K\,T_p \quad .....1.5$$

Therefore, equation 1.4 becomes

$$\frac{\partial^2 V(x,y,t)}{\partial x^2} + \frac{\partial^2 V(x,y,t)}{\partial y^2} = -\,K\,J_c(t) \quad .....1.6$$

For the sinusoid steady state

$$V(x,y,t) = V(x,y)e^{j\omega t} \quad .....1.7$$

and $$J_c(t) = J_c\, e^{j(\omega t + \theta)} \quad .....1.8$$

where $\theta \simeq -\frac{\pi}{2}$ because of the large ratio of capacitive-coupling reactance to equivalent surface resistance. On substitution of equation 1.7 and 1.8 into 1.6 there results

$$\nabla^2 V(x,y) \simeq -\,K\,J_c \angle -90^\circ \quad .....1.9$$

As shown in Appendix A, the time varying magnetic vector potential $A_z(x,y,\omega)$ satisfies the Poissonian equation.

$$\nabla^2 A_z(x,y,\omega) = - \mu_o \mu_r J_z(x,y,\omega)$$

When $\omega = 0$, one has

$$\nabla^2 A_z(x,y) = -\mu_o \mu_r J_z \qquad .....1.10$$

Therefore, lines of constant magnetic vector potential or flux lines are directly analogous to equipotential lines on the conducting paper surface (orthogonal analogue). The resistance per square of the paper analogues the permeability of the magnetic system. The dc current density J_z corresponds to the uniformly-distributed capacitive current density J_c.

A transformer circuit allows the location of equipotentials on the Teledeltos surface by a null technique. The circuit shown in Figure 1:4, is simple but very effective.

A voltage is developed across the resistance R which is exactly equal in amplitude and phase to the maximum voltage on the Teledeltos surface, the kernel voltage V_k. The vernier amplitude and phase adjustment is controlled by R' and C' respectively. The resistance R can be set at any percentage value of V_k. If the map current increases slightly due to coupling-capacitor drift, the voltage across

R will also increase due to transformer action. The circuit, is therefore, self compensating for map capacitive drift. A differential amplifier serves as the null detector. The accuracy of flux line location, essentially limited by the slight anisotropy of the Teledeltos medium, is approximately 1%.

1.2.4 AC Capacitively-Coupled Multiple Source Analogue

In 1965, S.I. Lourie[7,8] of the U.S.S.R. demonstrated a capacitively-coupled analogue for the magnetic vector potential of a multiple uniformly-distributed source field. This analogue was used, in application, to map the leakage field of a power transformer.

The Lourie analogue system uses a glass dielectric. The conducting paper is held tight against the dielectric by a layer of crushed non-conducting porcelain. (When plotting flux lines on the paper surface, the crushed porcelain is merely brushed away in the area of interest.) This weighted-layer method of keeping the paper against the glass is preferred for two important reasons:

(a) It is practically very difficult to glue large sheets of conducting paper onto the glass dielectric.

(b) The use of glue causes the conducting paper to become inhomogeneous leading

to large errors in flux line location.

The source regions are aluminum foil cutouts glued and rolled smooth onto the bottom side of the glass dielectric. Because the glass dielectric has appreciable thickness, e.g. 0.2 cm, there is a fringing electric field at the perimeter of the source regions. For this reason, the aluminum foil cutouts are sent back from the true source outline by a factor of $0.65T_d$, where T_d is the thickness of the glass dielectric.

The foil electrode couples capacitive displacement current into the conducting paper. The frequency is so low that the capacitive displacement current density over each source region is constant for all practical purposes. For each capacitively-coupled region the Poissonian equation $\nabla^2 V(x,y) = -KJ_{ci}$ applies. The surface voltage distribution $V(x,y)$ must also satisfy $\nabla^2 V(x,y) = 0$ outside any source region.

The current into each electrode is controlled using a series capacitance. An electrode current is measured by switching in series a large capacitance. The voltage drop across this capacitance is very small compared to that across the equivalent electrode capacitance. It is conveniently measured using a V.T.V.M.

In order to make voltage measurements on the conducting

paper it is necessary to use a "Wagner Earth" circuit. This circuit allows any point on the map surface to be brought to virtual ground potential. This procedure minimizes stray capacitive leakage currents due to:

(a) surface voltage measurement

(b) hand capacitance effects

On the map surface, equipotential lines correspond to lines of constant magnetic vector potential or flux lines. To plot an equipotential the following procedure is used:

(a) Some point on the conducting paper is brought to virtual ground potential.

(b) An ac differential milli-voltmeter is used to locate several points of the same potential with respect to ground.

(c) One of these points is now connected to one of the milli-voltmeter inputs. With the hand probe connected to the other input, the equipotential can now be located using the milli-voltmeter as a null indicator.

Differential voltages at any point on the map surface represent the equivalent flux density at the corresponding point in the magnetic system. Consider a flux density component in the x-direction, i.e. $B_x(x,y)$. It is given in terms of the magnetic vector potential by

$$B_x(x,y) = \frac{\partial A_z(x,y)}{\partial y}$$

or

$$B_x(x,y) = \lim_{\Delta y \to 0} \frac{A_z(x,y+\Delta y) - A_z(x,y)}{\Delta y} \qquad .....1.11$$

In the analogue system one has

$$\Delta V_x(x,y) = \lim_{\Delta y \to 0} \frac{V(x,y+\Delta y) - V(x,y)}{\Delta y}$$

or

$$\Delta V_x(x,y) \simeq \frac{V(x,y+\frac{\Delta y}{2}) - V(x,y-\frac{\Delta y}{2})}{\Delta y} \qquad .....1.12$$

if Δy is small compared to the x and y-dimensions of the map. An ac differential milli-voltmeter is used in conjunction with a double probe to measure analogous values of flux density. As shown by equation 1:12 the probe points must be aligned at 90° to the flux density vector to be measured. The milli-voltmeter employs a transistor design with a high differential input impedance and a floating power supply (battery).

The essential Lourie system is shown in Figure 1:6.

1.3 Scope of the Thesis

This thesis describes a new capacitively-coupled multiple source analogue system. A new analogue map is detailed. The use of a thin tape dielectric instead of a glass dielectric is shown to be both theoretically and

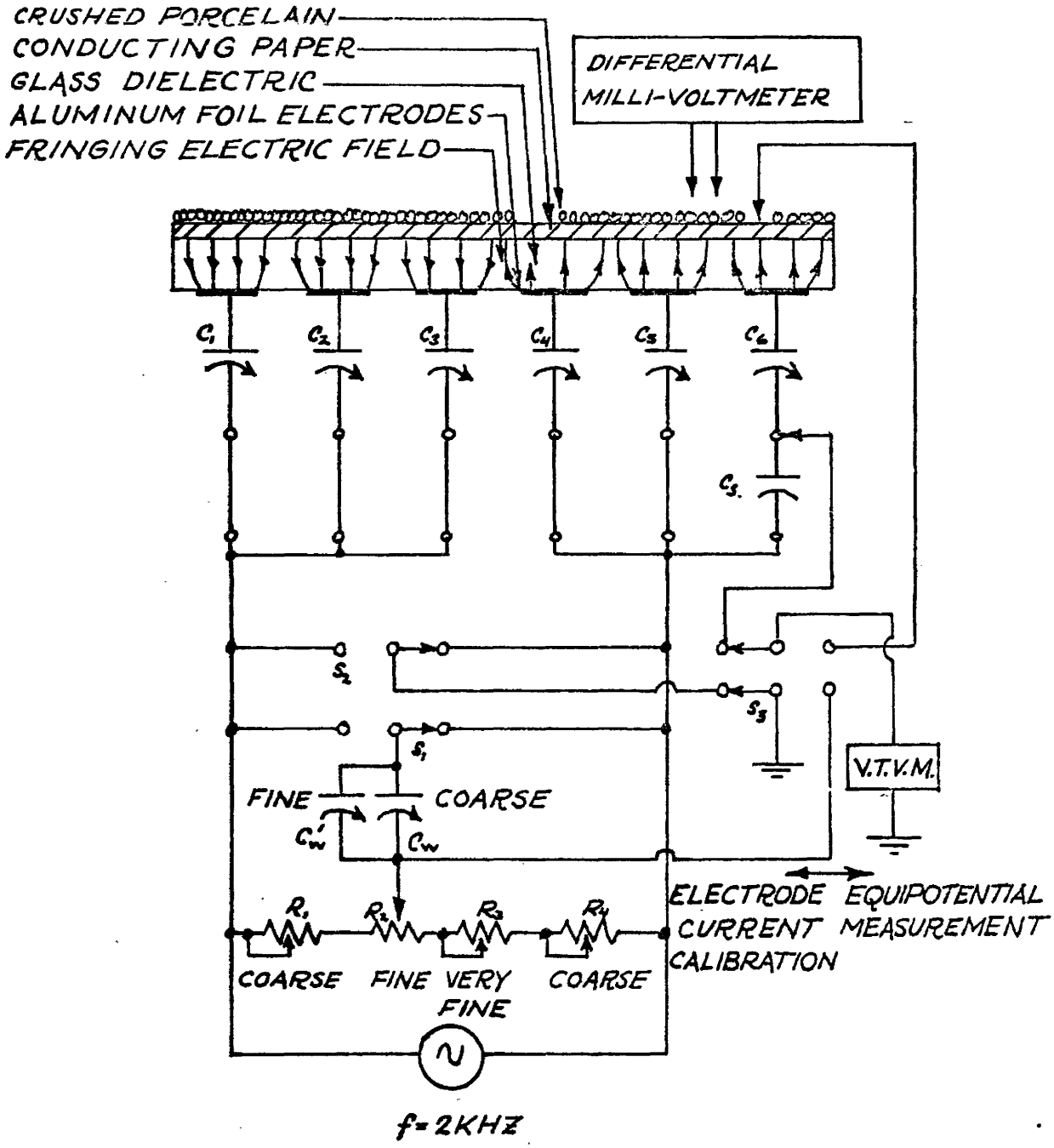

FIGURE 1.6 THE LOURIE MULTIPLE SOURCE ANALOGUE

practically advantageous. A method of connection to the capacitively-coupled electrode has been developed which allows the creation of a physically flat map. A simple and efficient null technique has been devised to locate equipotentials on the map surface in percentage values. The system circuitry compensates for equipotential variation due to coupling-capacitance drift. The null detector is a linear amplifier (OP-AMP design) with a dual FET differential input and a dc voltage readout. This differential voltmeter in conjunction with a double probe gives field density information at any point on the map surface.

Experimental results are given which illustrate the accuracy and versatility of the system. The flux line and flux density distribution accuracies are defined in terms of a circular conductor in free space carrying direct current.

A generalized theory of the capacitively-coupled analogue is given. The theory suggests a two-dimensional analogue to simulate the magnetic vector potential from sources in which skin effect is present. A demonstration of the new skin effect analogue is given.

A new mapping system is suggested which can analogue the magnetic vector potential of multiple sources when the sources have controllable magnitude and phase with respect

to each other at any frequency. This analogue could map the instantaneous magnetic flux distribution of a system of conductors carrying three phase currents.

CHAPTER 2

2.1 An Improved Capacitively-Coupled Map

The capacitively-coupled Poissonian analogue maps discussed in Chapter 1 suffer from a number of disadvantages. The procedure of gluing a large sheet of Teledeltos paper to the glass dielectric can be cumbersome. Aside from this, the adhesive usually impregnates the Teledeltos medium. The resistance per square of the paper now becomes variable so that $K \rightarrow K(x,y)$. In regions where $K(x,y)$ deviates greatly from K, the surface voltage distribution $V(x,y)$ can be substantially in error. It is for this reason that the Lourie map construction technique employs a layer of non-conducting porcelain to hold the conducting paper onto the glass. For flux plotting or flux density measurement purposes, the crushed porcelain must be brushed away in the area of interest on the conducting-paper surface. Although this method produces a voltage distribution of better accuracy, it still has this unwieldy aspect.

The glass dielectric used in previous maps can have appreciable thickness; typically $T_d \approx 2mm$. As such, the fringing electric field at the perimeter of a coupling electrode is not negligible. This fringing field produces an error current in the conducting paper in an area just

around the electrode perimeter. This current, in turn, causes the surface voltage distribution V(x,y) to be incorrect in and around the same area. The erroneous effect of this fringing electric field can be compensated for by setting the electrode perimeter back from its original position by a distance δT_d metre. Lourie derived a value for the factor δ from a field plot of the fringing electric flux in the dielectric when $\varepsilon_r = 7$. He reports that $\delta = 0.65$.[7]

The fringing electric field may be entirely neglected if the glass is replaced by a thin tape dielectric.[9] A dielectric can be defined to have an effective thickness given by

$$T'_d = \frac{T_d}{\varepsilon_r}$$

Thus, the effective thicknesses of the tape and glass dielectrics are given respectively by

$$T'_t = \frac{T_t}{\varepsilon_t} \quad \text{and} \quad T'_g = \frac{T_g}{\varepsilon_g}$$

If the ratio of the effective thicknesses is such that $\frac{T'_t}{T'_g} \leq \frac{1}{10}$ then the fringing field can be considered practically negligible. That is, it would be useless to locate the perimeter to within δT_t because T_t itself would typically be 0.1 mm. The fringing electric field in the glass and tape dielectrics is shown in Figure 2:1.

GLASS DIELECTRIC SYSTEM

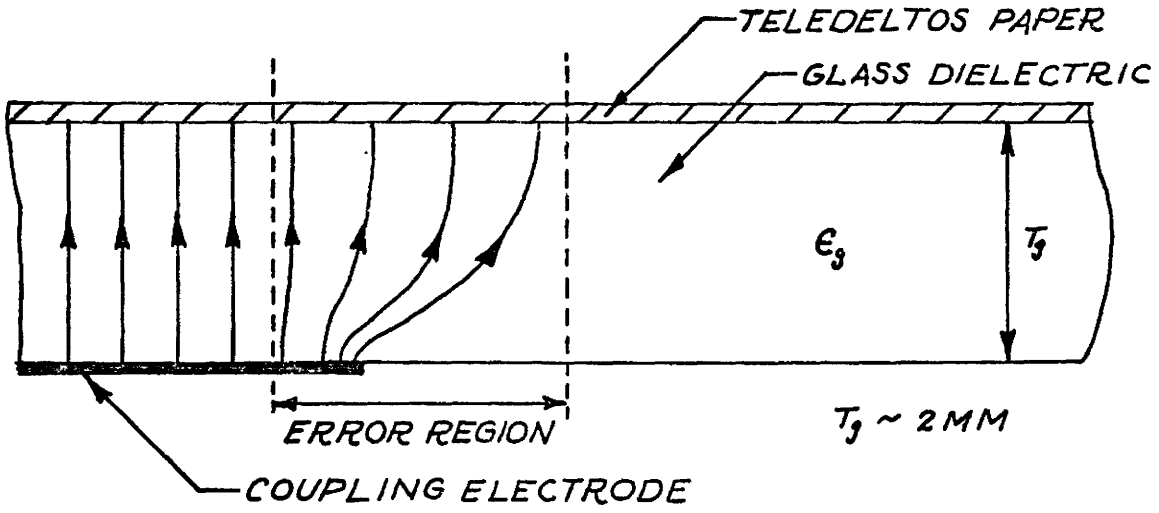

TAPE DIELECTRIC SYSTEM

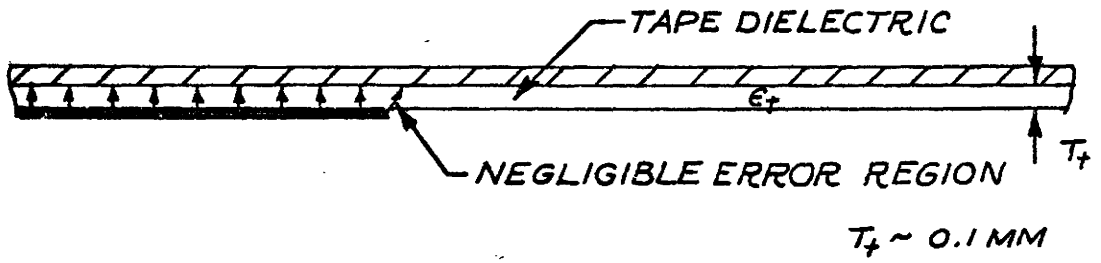

FIGURE 2.1 FRINGING ELECTRIC FIELD AT ELECTRODE PERIMETER

The thin layer of dry pressure-sensitive adhesive on the tape dielectric does not impregnate the conducting paper. Therefore, the resistivity of the Teledeltos paper remains unchanged. To ensure a constant displacement current density over the whole coupling electrode area, the capacitance per unit area of an electrode must be constant, i.e.

$$C'_e = \frac{\epsilon_o \epsilon_r}{T_d} = \text{a constant}$$

Hence, the tape dielectric should possess a constant permittivity and thickness.

The use of aluminum foil as coupling electrodes is questionable. The foil must be carefully cut to the exact electrode geometry, a special adhesive applied to one side, and then positioned accurately on the dielectric. Subsequently, the foil is rolled smooth so that no air is trapped. When a tape dielectric is used it is advantageous to paint an electrode on to it, using conducting silver paint. Although more expensive than aluminum foil, silver paint allows complicated electrode shapes to be formed with comparative ease.

A method of connection to each silvered electrode which is simple and effective was sought. A procedure has been developed which permits the electrical connection to lie in the plane of the conducting paper.[9] Connection is made from the edge of the map to a given silvered electrode area using a thin strip of copper tape symmetrically

positioned on a dielectric tape strip. For any copper strip, the effective coupling capacitance per unit area to the conducting paper can be expressed as

$$C'_s = \frac{\varepsilon_o \varepsilon_s}{T_s} \qquad F/m^2$$

where ε_s is the relative dielectric constant of the tape strip and T_s is its thickness in metres. If the ratio between the effective coupling capacitance per unit area of a copper strip and a silvered electrode is,

$$\frac{C'_s}{C'_e} = \frac{\varepsilon_s \, T_d}{\varepsilon_r \, T_s} \leq \frac{1}{10}$$

then, the copper strip is essentially decoupled capacitively from the conducting paper surface. Actual connection between the copper tape and the electrode area is accomplished by painting over the junction with silver. At the other end, the copper strip is brought past and bent around an extension of the dielectric tape strip to form a tab. Wire may be soldered directly to this tab. When all the necessary construction materials are at hand, a map of ordinary complexity can be constructed in about two hours. The map fabrication technique is illustrated in Figure 2:2.

2.2 A New Method of Equipotential Location[9]

The magnetic vector potential of a multiple source field will contain at least one point of zero flux density. Usually, there are two such points although some magnetic

CROSS-SECTION OF COUPLING ELECTRODE CONNECTION

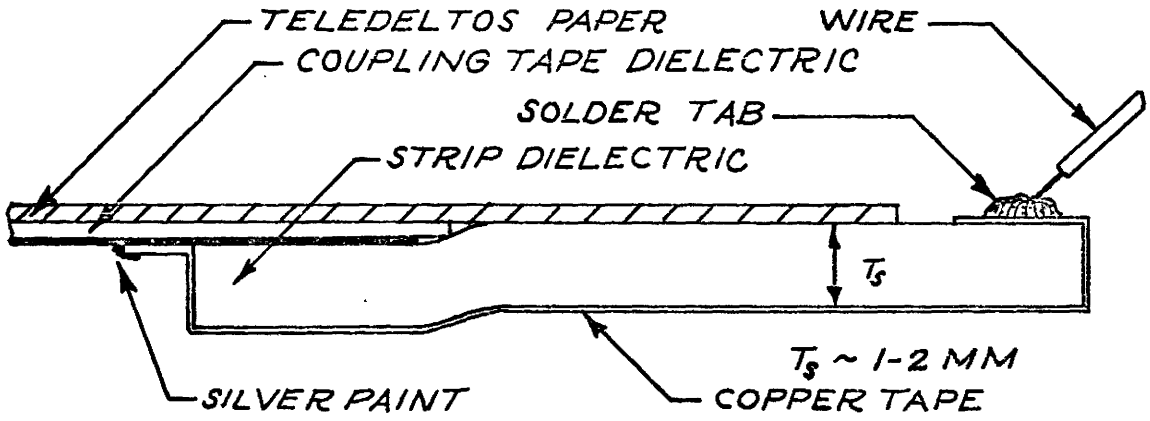

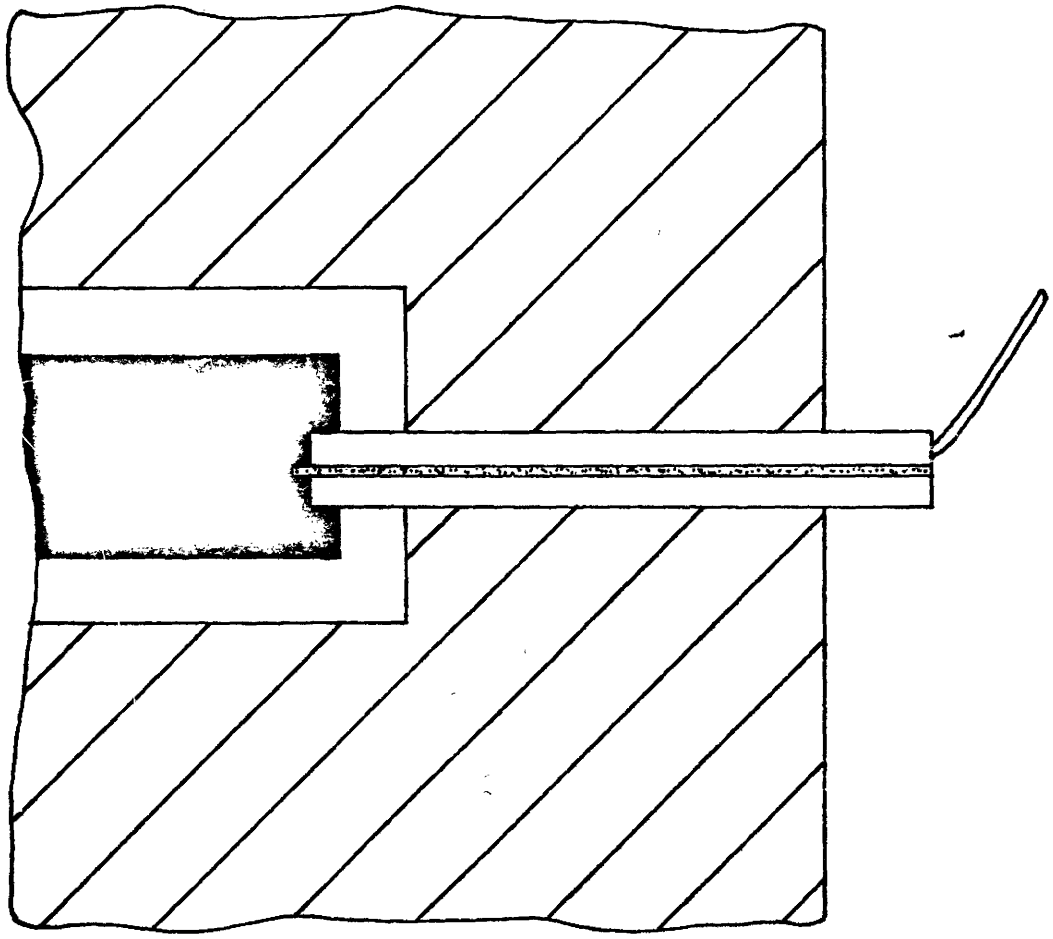

FIGURE 2.2 MAP CONSTRUCTION

field distributions have more. These different types of field distributions are illustrated in Figure 2:3.

In a magnetic field distribution which has two points of zero flux density, the total flux is contained between them. This field type is perhaps the most commonly plotted two-dimensional distribution. These points of zero flux density in the magnetic system correspond to kernel points on the map. A kernel point is one of two unique points of the map which exhibit a maximum voltage difference between them. All the equipotentials essential in defining the flux distribution exist between these two points. If exactly the kernel to kernel voltage in amplitude and phase can be created across a linear calibrated potentiometer, the equipotentials may be located using a null technique. The circuitry for the system is shown in Figures 2:4 and 2:5.

2.2.1. "Wagner Earth" Circuit.

The "Wagner Earth" circuit allows any point on the map surface to be brought to virtual ground potential. The intrinsic characteristic of this new equipotential plotting method is that one of the kernel points must be brought to virtual ground potential. This procedure implies two very important considerations:

(a) That one of the kernel points may be used as a ground reference; and

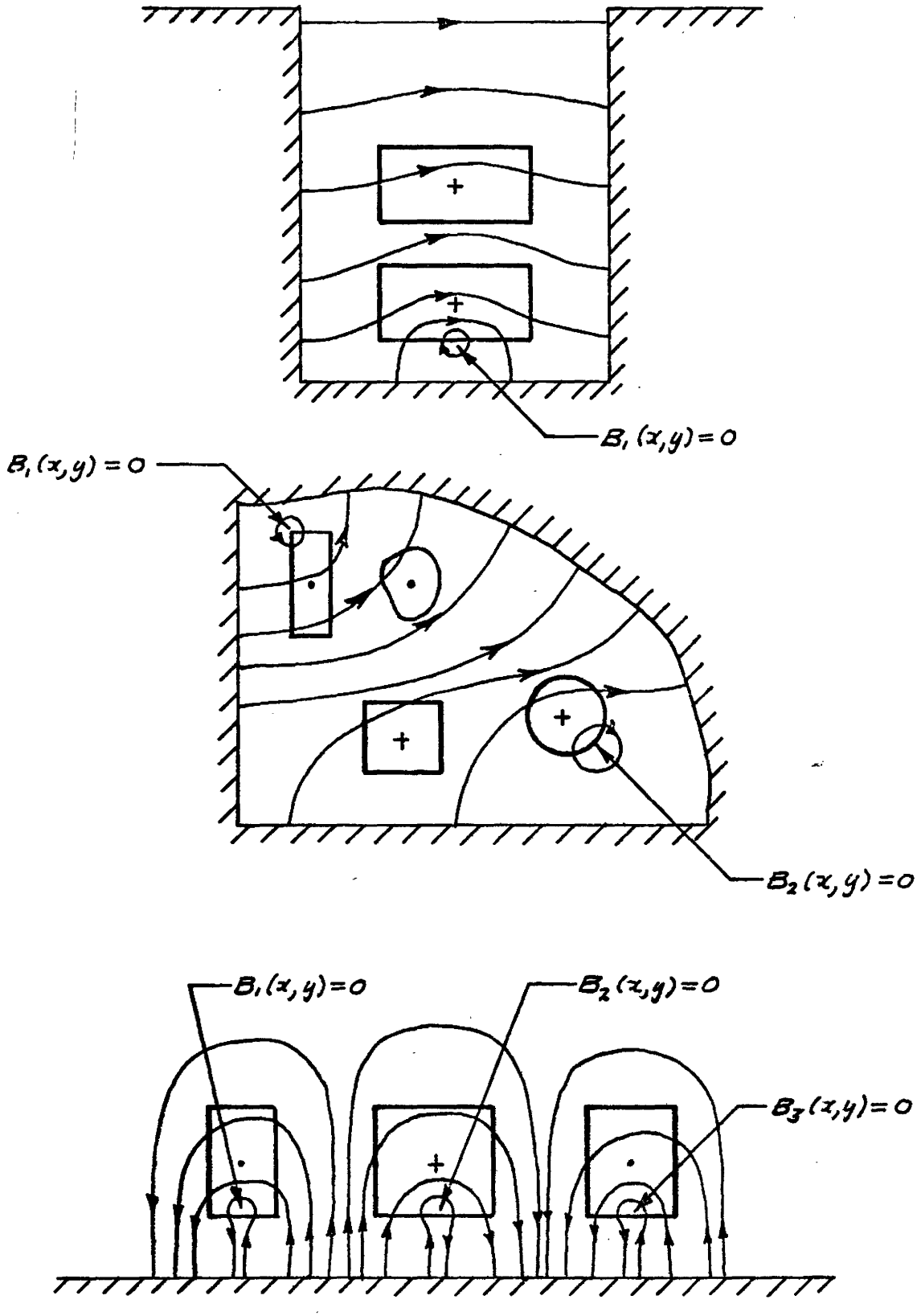

FIGURE 2.3 DIFFERENT MAGNETIC FIELD DISTRIBUTIONS

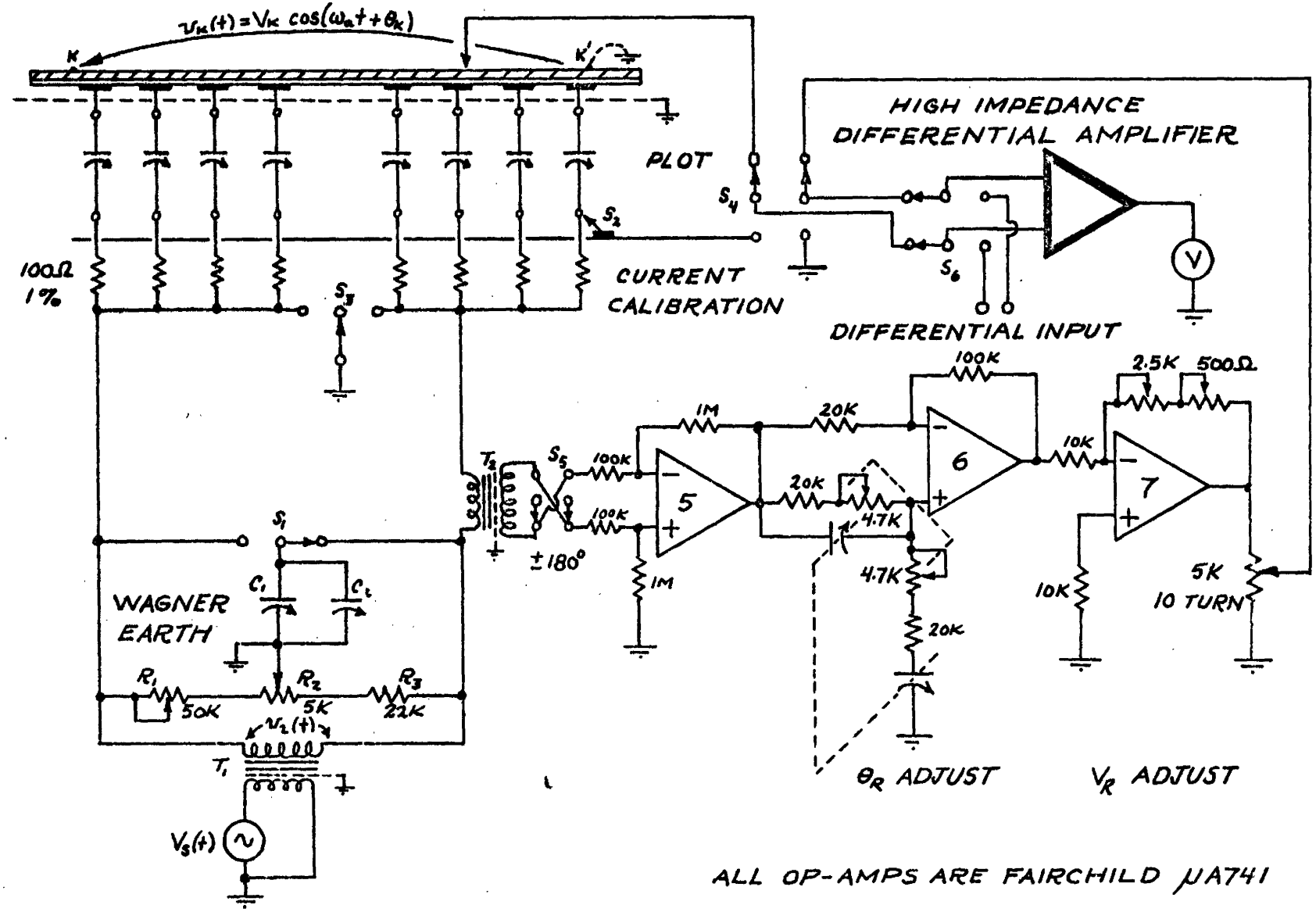

FIGURE 2.4 ANALOGUE CIRCUITRY

ALL OP-AMPS ARE FAIRCHILD μA741

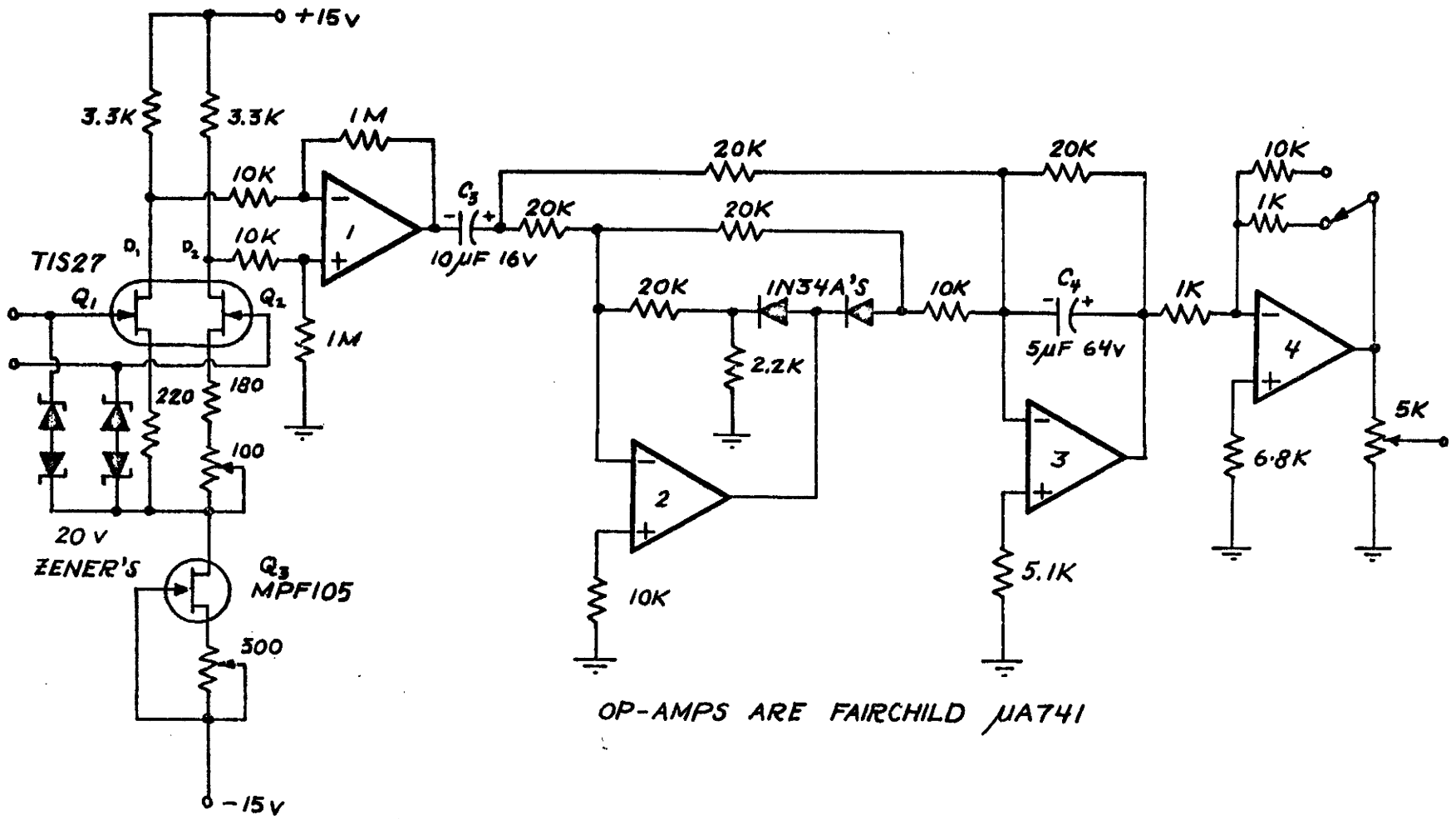

FIGURE 2.5 HIGH IMPEDANCE VARIABLE GAIN DIFFERENTIAL AMPLIFIER

(b) That having a virtual ground potential on the map surface minimizes ground leakage currents which could cause a large distortion in the field pattern.

These distorting map leakage currents can exist if the map surface is at a reasonable potential above ground (A leakage current could flow, for example, through the plotting probe to ground). However, the kernel to kernel voltage is very small in comparison to the map excitation voltage because of the large ratio of any coupling capacitive reactance to the equivalent surface resistance. Hence, map surface leakage currents are practically non-existent.

The "Wagner Earth" circuit physically consists of resistors R_1, R_2, and R_3 and capacitors C_1 and C_2. The variable capacitors C_1 and C_2 can be switched from one side of the resistive arm to the other using S_1. The coarse and fine controls facilitate easy and rapid placement of a virtual ground on the map surface. The effective loading impedance of the circuit across transformer T_1 is minimal so that the secondary voltage $v_2(t)$ remains essentially unaffected with adjustment of R_1, R_2, C_1 and C_2.

2.2.2. Coupling Electrode Current Control

The current flowing into each electrode of the map is controlled by a series capacitor. The control capacitor allows

stepped and vernier adjustment of the individual electrode current. In series with each control capacitor, a resistor has been placed in order to measure the relative value of coupling capacitor current. Each resistor is of the same low ohmic value (100Ω) such that the voltage drop is very small in comparison with that across each equivalent electrode capacitance.

Switch S_2 selects which relative electrode current is to be measured. The voltage across the corresponding resistor can be measured with the differential voltmeter when a ground potential exists on the resistor common. Switch S_3 can bring either of the two resistor commons to ground potential. This method supposes changing the ground potential from one side of T_1's secondary to the other in no way affects the secondary voltage $v_2(t)$. This assumes T_1 to be a symmetrically wound transformer with a grounded electrostatic shield.

2.2.3 The Reference Voltage Circuit

This circuit develops a voltage exactly in amplitude and phase to the kernel to kernel voltage when one of the kernel points is at virtual ground potential. The kernel to kernel voltage can be expressed as $v_k(t) = V_k \cos(\omega_a t + \theta_k)$ volts. The amplitude and phase (refer to Appendix B) of the reference can be adjusted independently so that the output

voltage $v_r(t) = V_r \cos(\omega_a t + \theta_r)$ can be made such that $V_r = V_k$ volts and $\theta_r = \theta_k$ radians. The high input impedance differential voltmeter is used as a null detector in conjunction with a hand probe to locate equipotentials.

The reference voltage $v_r(t)$ is derived from the total map current. If the effective coupling reactance changes due to temperature affecting the tape dielectric, the reference voltage will change proportionately. The circuit therefore, compensates for coupling capacitor drift. The drift can affect the accuracy of equipotential location. The effective primary impedance of the coupling transformer T_2 is very small in comparison with the equivalent coupling reactance. Transformer T_2 also has electrostatic shielding to provide adequate isolation.

To ensure low distortion the circuit utilizes modern monolithic IC operational amplifiers - Fairchild type μA741. Low distortion is important when two voltages are being compared since equipotentials will be located more accurately by the circuitry if deep nulls are possible.

2.2.4 The High Impedance Differential Amplifier

The ac differential amplifier shown in Figure 2:4 and Figure 2:5 serves as:

(a) a null detector for the placing of a virtual ground on the map surface

(b) a null detector for the location of equipotentials on the map surface

(c) a linear variable-gain amplifier for the measurement of small voltages across the 100Ω current calibration resistors

(d) a linear variable-gain amplifier for the measurement of very small differential voltages on the map surface.

The circuit employs a dual FET differential input stage (Q_1, Q_2). The Zener diodes protect the dual FET in case the hand probe or the differential probe punctures through the Teledeltos-dielectric sandwich to an electrode. The Zener diodes also provide return paths for the gate-to-source reverse leakage currents of Q_1 and Q_2. The differential input impedance is greater than 1MΩ.

The FET differential stage is designed for low distortion. With FET (Q_3) employed as a current source, the common mode rejection ratio (CMMR) of the input stage is enhanced. The input differential signal, amplified approximately fifteen times, appears between drain terminals D_1 and D_2. The differential voltage is converted to a single ended signal with a gain of 100 by OP-AMP #1. The signal is now coupled to a standard precision operational amplifier ac-to-dc converter via capacitor C_3. The dc output of the converter is amplified by the variable gain

configuration of OP-AMP #4. This configuration offers gains of 1 and 10. The 5KΩ potentiometer at the output allows the voltage to be scaled to any relative value. The output voltage may be read on any analogue or digital voltmeter of high input impedance.

Switches S_4 and S_6 in combination control the amplifier's use as either a null detector for equipotential location, or as a differential voltage amplifier for measuring analogous values of flux density. With S_4 in a plot position, the hand probe is made operational. The hand probe is connected via a grounded shielded cable through a BNC type connector on the instrument panel to the circuitry inside. The other amplifier input terminal is connected to the wiper on the precision reference voltage potentiometer. In S_6's other position, the amplifier can be employed as a differential voltmeter. In this position, the amplifier input terminals are connected to two universal binding posts on the instrument panel. A twisted pair cable is used to connect a double probe to the binding posts. The double probe shown in Figure 2:6 is used to measure small differential voltages on the map surface. The probe point spacing is approximately 4 mm. The probe points are rigidly glued to the plastic protractor to minimize measurement error due to movement. The clear plastic protractor allows the probe points to be aligned at any angle with respect to guide lines drawn on the map surface. The probe points must be aligned at 90° to the vector

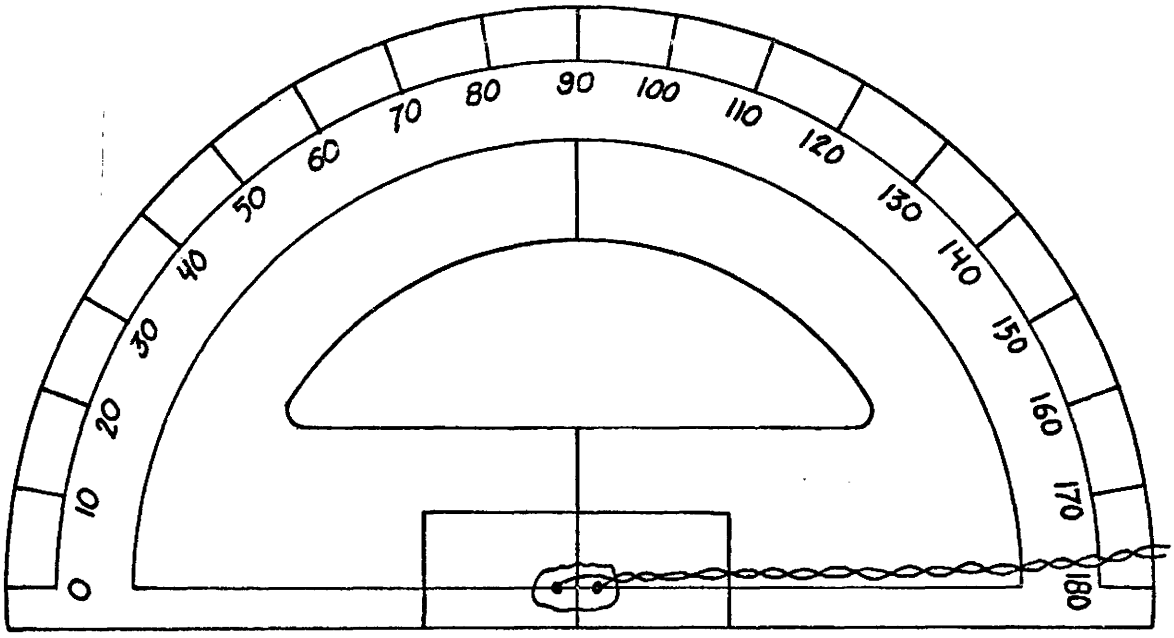

PROBE CROSS-SECTION

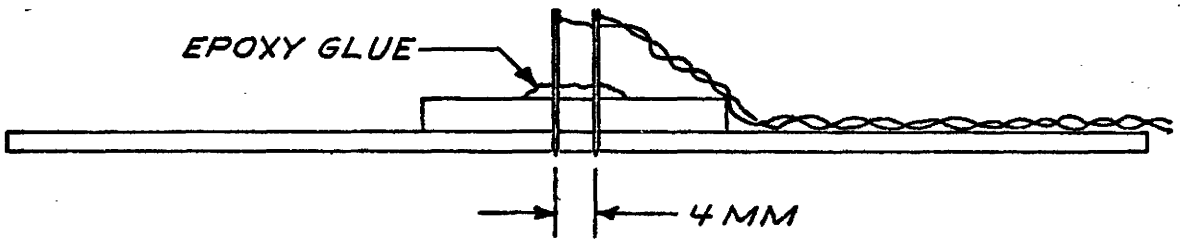

FIGURE 2.6 PROTRACTOR DOUBLE PROBE

whose magnitude is desired.

2.2.5 The Guard Electrode

A grounded guard electrode is placed on the bottom side of the map. This grounded conducting surface minimizes:

(a) 60 Hz pickup on the map surface

(b) any stray coupling electrode electric flux.

The effective capacitance between the map surface and the guard electrode is very small since:

(a) the map surface voltage drop is very small and almost at ground potential (Wagner Earth)

(b) the separation between the map surface and the guard electrode is approximately 2 cm.

Therefore, no capacitive leakage currents are induced on the map surface which could cause equipotential distribution distortion. The guard electrode is shown in Figure 2:7.

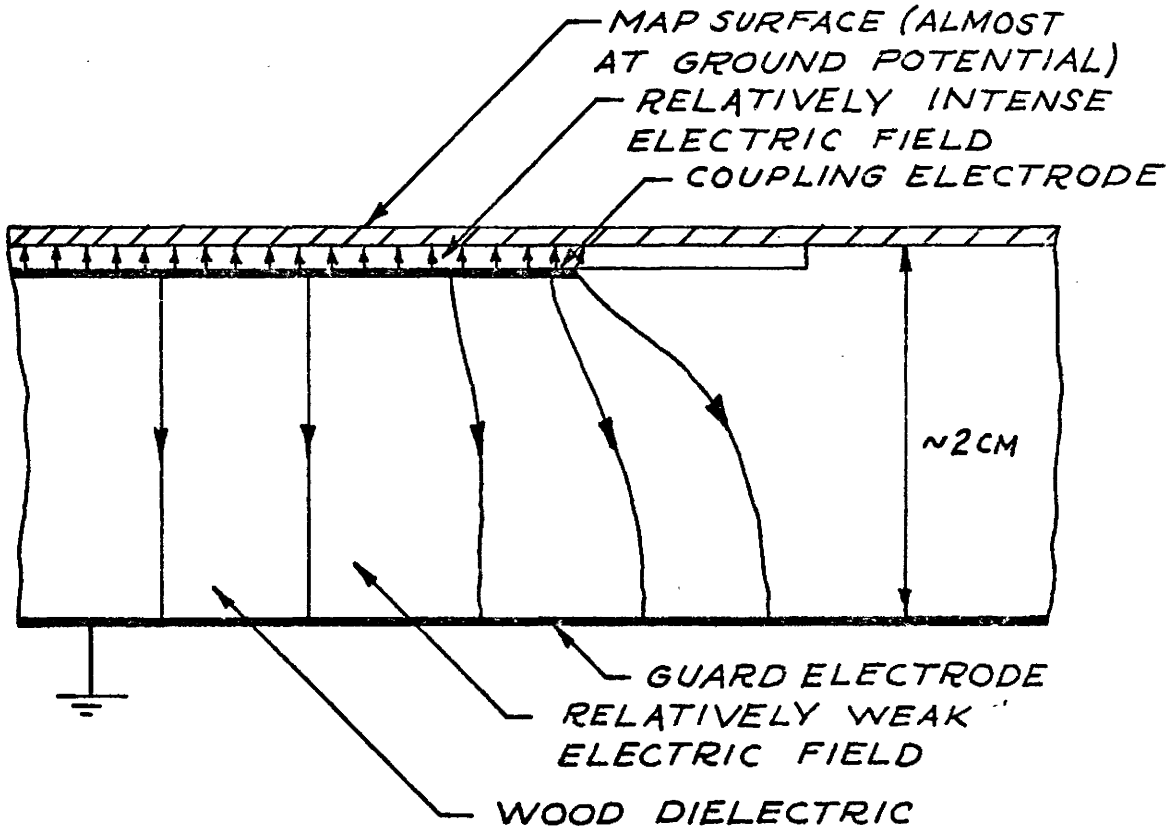

FIGURE 2.7 THE GUARD ELECTRODE

CHAPTER 3

3.1 Field Plotting Accuracy

Sources of possible error in realizing a desired equipotential distribution on the map surface can be listed as follows:-

(a) finite surface voltage drop; in order to plot an equipotential distribution a small voltage drop must exist across the map surface. Since the supply voltage to the map electrodes is usually greater than one hundred times the surface voltage drop, the effect of this error is negligible.

(b) inhomogeneity of the conducting paper; the Teledeltos manufacturing process introduces a directional anistropy in the paper. The difference in the two resistivites (90° apart) can be as much as 10%. The effect of the directional resistivities on the equipotential distribution can be corrected for as shown in Appendix C. The paper resistivity can be affected by humidity variations. The paper is relatively unaffected by temperature variations if its moisture content is small. A typical temperature coefficient is -0.2%/°C.

(c) inhomogeneity of the dielectric; the capacitive displacement current density can vary over the area of a coupling electrode if dielectric thickness or the relative

permittivity ε_r varies. Depending on the dielectric used, the effective coupling capacitance of an electrode may vary with temperature (e.g. polyethylene has a temperature variation of -0.01%/°C).

(d) electrode boundary fringing electric field; the fringing electric field along the perimeter of an electrode creates an error current. The error current that enters the paper along an electrode boundary becomes insignificant when the thickness of the dielectric is negligible compared with the x and y dimensions of the electrode.

(e) measurement and map circuitry; the measurement technique used to locate an equipotential depends upon precise waveform processing with low distortion by active circuitry. The linearity of the precision potentiometer that is the basis of the null technique is of direct importance.

(f) coupling capacitance of connection strip; a coupling capacitance is formed between a copper connection strip and the map surface. This capacitance is very small in comparison with source electrode coupling capacitances. Therefore, any error currents introduced into the map surface are believed to have little effect on the surface voltage distribution.

(g) coupling capacitance of guard electrode; the grounded guard electrode offers a fixed capacitance to the map surface.

This coupling capacitance is very small and its effect should not be significant.

The cumulative inaccuracy of the surface voltage distribution from all the sources of error can be simply determined. Figure 3:1 shows the cross-section of a circular conductor in free space carrying dc. The tangential flux density from the centre of the conductor ($r = 0$) to the outside surface ($r = r_o$) is given by

$$B_1(r) = \frac{\mu_o I}{2\pi r_o^2} r \qquad \text{teslas} \qquad 0 \leq r \leq r_o$$

Outside r_o, the tangential flux density is given by

$$B_2(r) = \frac{\mu_o I}{2\pi r} \qquad \text{teslas} \qquad r_o \leq r < \infty$$

The total flux per unit length of conductor contained between $r = 0$ and $r = 3r_o$ is

$$\phi'_{03} = \int_o^{r_o} B(r)\, dr + \int_{r_o}^{3r_o} B(r)\, dr = \frac{\mu_o I}{2\pi} \left[\tfrac{1}{2} + \ln 3\right] \text{ webers/m.}$$

The values of flux per unit length calculated in 20% intervals as a function of radius r are given in Table 1. The analogue equivalent of this conductor configuration was constructed. As shown in Figure 3:1 the source electrode connection strip has been included in the map construction. The flux plotter was used to obtain the corresponding equipotentials in percentage values at the calculated radii.

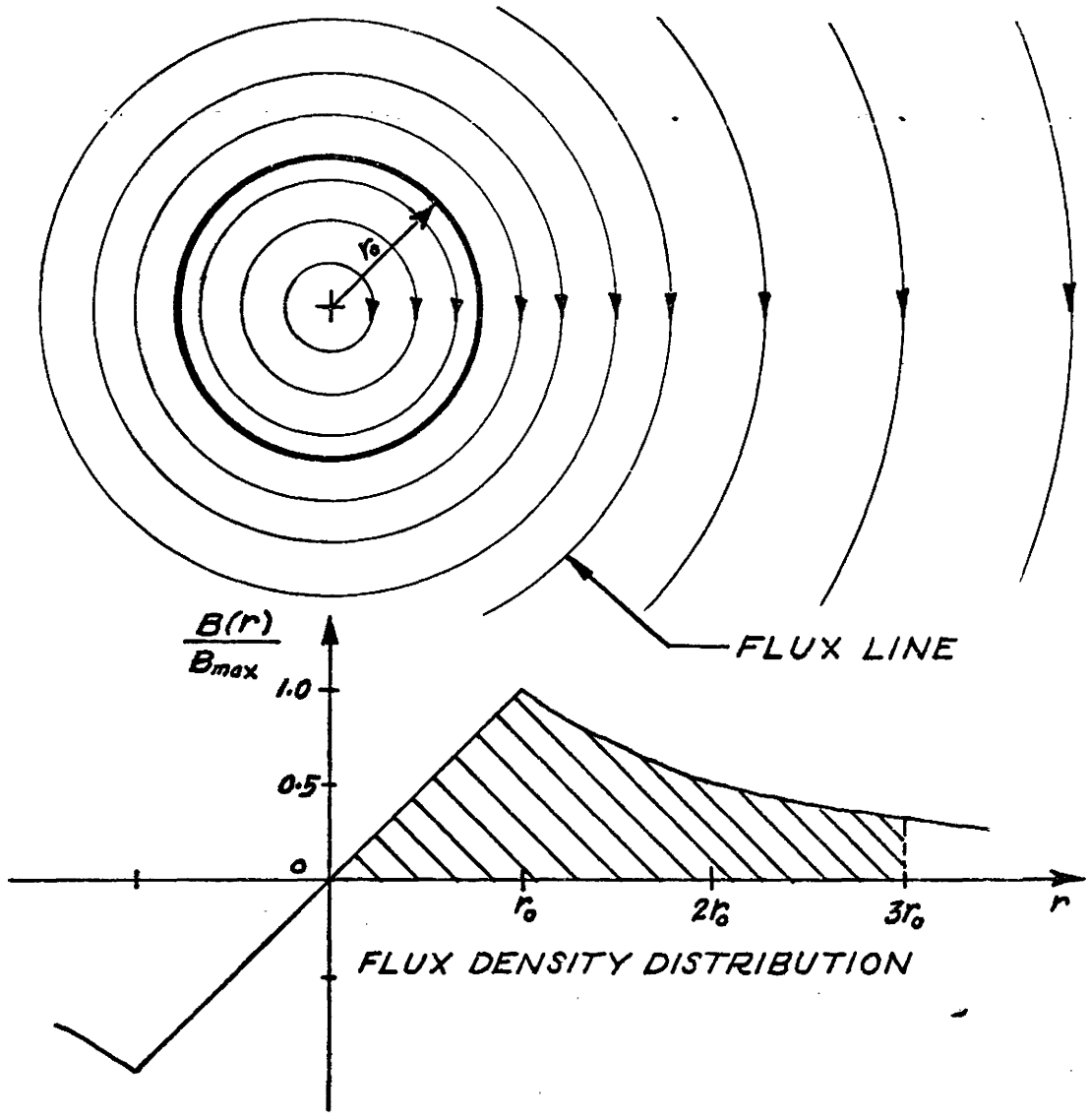

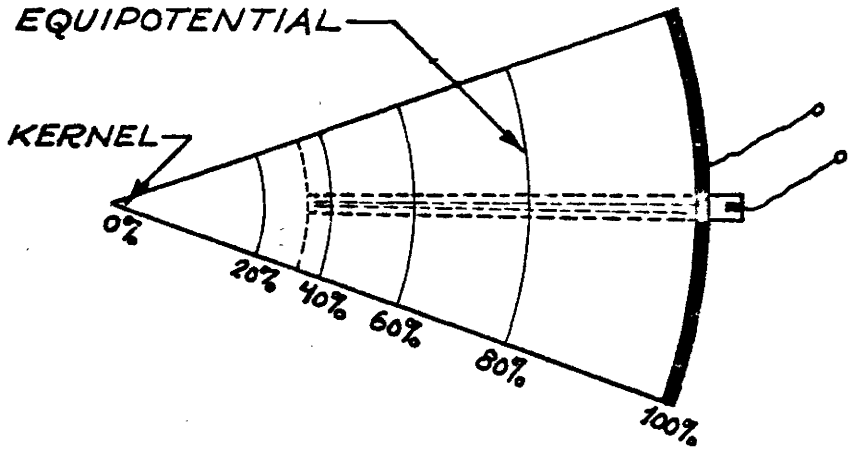

FIGURE 3.1 CIRCULAR CONDUCTOR AND ANALOGUE EQUIVALENT

The equipotential values and their percentage deviation are shown in Table 1.

r metres	$\frac{\phi'(r)}{\phi'_{03}}$	$\frac{V(r)}{V_k}$	% Deviation
0	0%	0%	-
0.8	20%	19.6%	0.4%
1.15 r_o	40%	39.9%	0.1%
1.58 r_o	60%	59.3%	0.7%
2.18 r_o	80%	79.7%	0.3%
3 r_o	100%	100%	-

r_o = 0.152m

TABLE 1: Flux Line Accuracy

3.2 Flux Density Accuracy

The added sources of error in determining analogous values of flux density from the map surface can be stated as:

(a) linearity of the high impedance, variable gain, differential amplifier; the linearity of the constructed amplifier is shown in Figure 3:2. Its essential accuracy depends upon the precision ac-to-dc converter.

(b) probe point separation; if the differential voltage measured by the double probe at any point on the map surface is very small in comparison with the kernel voltage or the kernel-to-kernel voltage, the effect of a finite probe point

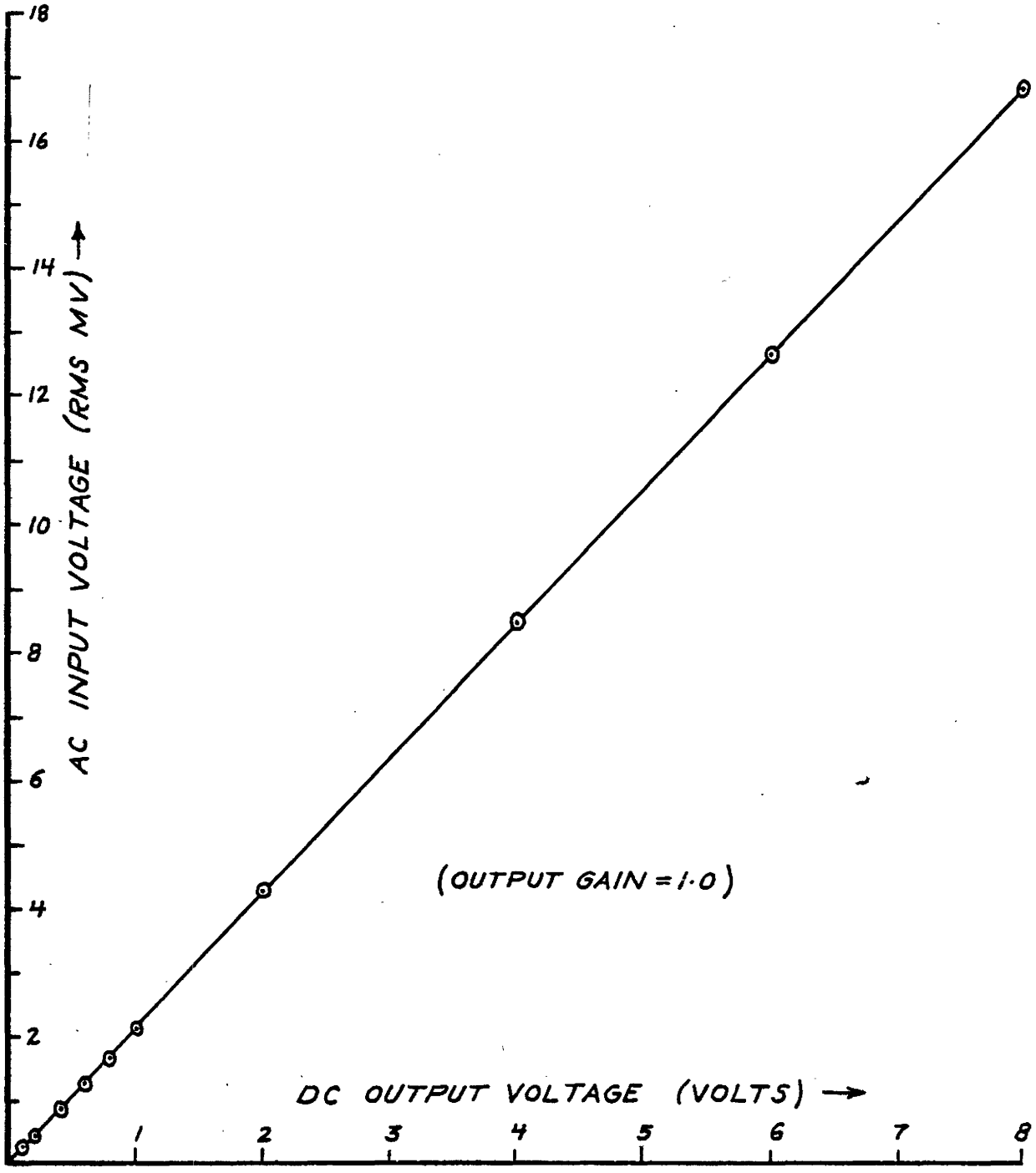

FIGURE 3.2 LINEARITY OF HIGH IMPEDANCE AC DIFFERENTIAL AMPLIFIER

separation becomes insignificant.

(c) alignment of the double probe; the probe points must be correctly aligned at 90° to the vector whose magnitude is to be measured. Alignment error essentially depends upon the operator.

Analogous values of flux density were obtained from the map shown in Figure 3:1. The normalized results are shown in Table 2.

r metres	Calculated $\frac{B(r)}{B_{max}}$	Measured $\frac{B(r)}{B_{max}}$	% Deviation
0	0.0	0.0	-
$0.25r_o$	0.25	0.25	0%
$0.50r_o$	0.50	0.48	2%
$0.75r_o$	0.75	0.76	1%
$1.00r_o$	1.00	1.00	reference
$1.25r_o$	0.8	0.80	0%
$1.50r_o$	0.667	0.67	<1%
$1.75r_o$	0.572	0.58	1%
$2.00r_o$	0.50	0.50	0%
$2.25r_o$	0.444	0.44	<1%
$2.50r_o$	0.40	0.39	1%
$2.75r_o$	0.364	0.34	>2%

TABLE 2: Flux Density Accuracy

3.3 Map Simplification

If symmetry exists in a magnetic field distribution, the equivalent analogue map may be simplified. Knowledge of the position of a certain flux line in a field distribution can also simplify a map. The resulting analogue maps usually have only one kernel point. This eases construction and enhances accuracy because of field magnification for a given maximum map size. These ideas are illustrated with the simple buss bar configurations shown in Figure 3:3.

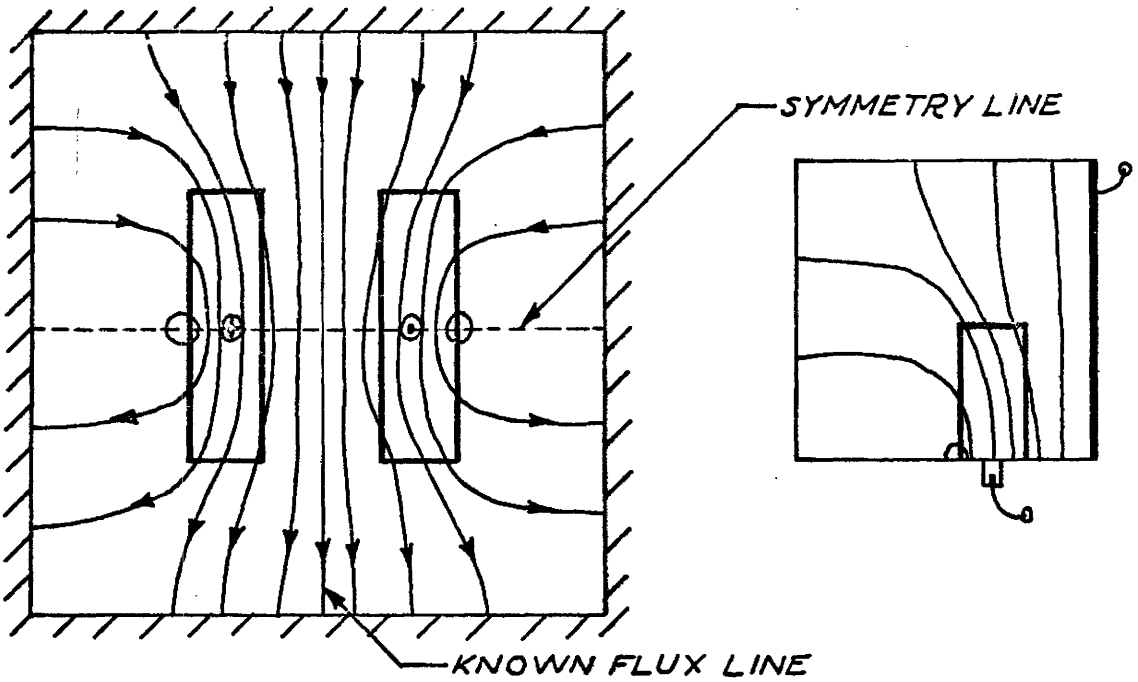

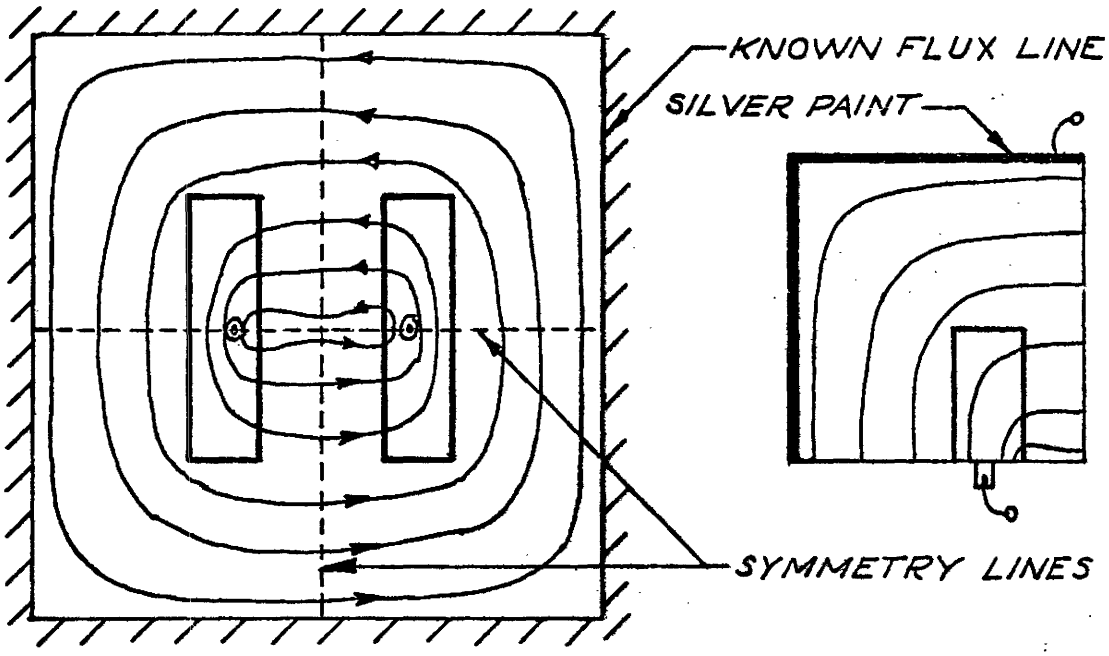

FIGURE 3.3 MAP SIMPLIFICATION

CHAPTER 4

4.1 Introduction

In this chapter the general equations of the analogue map are derived. In the first part, a general elemental equivalent circuit is used to represent an elemental section of the map. From an analysis of this equivalent circuit it is shown that the currents that flow in the plane of the conducting paper are independent of the dimensional variable z. This implies a simpler equivalent circuit.

From the new equivalent circuit the equation governing the capacitive current density distribution is derived. This equation is identical with the differential equation describing the current density distribution in a real conductor. General co-ordinates are introduced for the map equation to account for the assumed scale difference between the analogue and the real conductor dimensions. The equation relating the map frequency and the real frequency in terms of the parameters of the analogue and real conductor systems is derived. At this analogue frequency, the capacitive current density distribution is the same as the real conductor current density distribution.

From the same equivalent circuit, the equation governing the surface voltage distribution and the capacitive

current density distribution is derived. For consistency, the equation is then written in terms of the general map co-ordinates. This equation has the same form as that governing the magnetic vector potential and the current density distribution in a real conductor.

4.2 A General Elemental Equivalent Circuit

The elemental map section shown in Figure 1:5 can be represented by the elemental equivalent circuit of Figure 4:1. The elemental resistances R_x, R_y, and R_z are derived from

$$R = \rho \frac{\text{Length}}{\text{Area}} \quad \text{ohms.}$$

Thus $$R_x = \rho \frac{\Delta x}{\Delta y \Delta z} = \frac{KT_p \Delta x}{\Delta y \Delta z} \quad \text{ohms}$$

since the resistivity ρ can be expressed in terms of the thickness T_p and the resistance per square K of the conducting paper, that is,

$$\rho = KT_p \quad \text{ohm-metre}$$

Similarly $R_y = \frac{KT_p \Delta y}{\Delta x \Delta z}$ ohms and $R_z = \frac{KT_p \Delta z}{\Delta x \Delta y}$ ohms

The current flowing in the z direction through the elemental capacitance is given by

$$I_T(t) = \sum_{i=1}^{n} \Delta I_i(t) \quad \text{amperes}$$

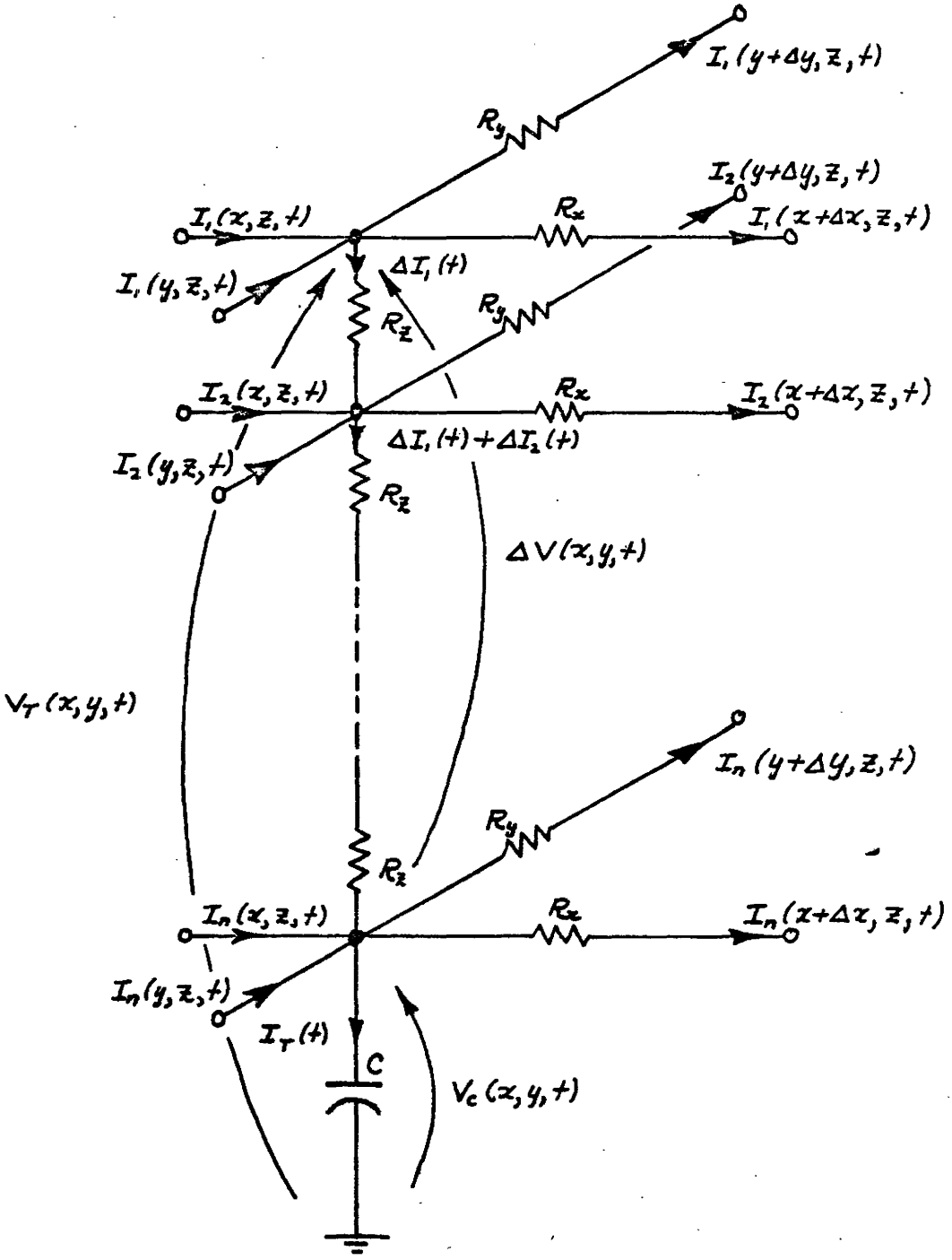

FIGURE 4.1 AN EQUIVALENT CIRCUIT FOR THE ELEMENTAL MAP SECTION

where

$$\Delta I_i = I_i(x,z,t) - I_i(x+\Delta x,z,t) + I_i(y,z,t) - I_i(y+\Delta y,z,t) \quad \text{amperes}$$

From the elemental equivalent circuit one has

$$V_T(x,y,t) = V_c(x,y,t) + \Delta V(x,y,t) \quad \text{volts}$$

or

$$\frac{V_T(x,y,t)}{V_c(x,y,t)} = 1 + \frac{\Delta V(x,y,t)}{V_c(x,y,t)} \qquad .....4.1$$

The quantity $\frac{\Delta V(x,y,t)}{V_c(x,y,t)}$ represents the error between the voltage from the datum to the top surface of the conducting paper $V_T(x,y,t)$ and the voltage from the datum to the dielectric paper interface $V_c(x,y,t)$.

The voltage developed across the elemental capacitance in the frequency domain is

$$V_c(x,y,\omega_a) = I_T(\omega_a) \frac{1}{j\omega_a C} = \frac{I_T(\omega_a)T_d}{j\omega_a \varepsilon_o \varepsilon_r \Delta x \Delta y} \text{ volts} \quad ...4.2$$

where the elemental capacitance is $C = \frac{\varepsilon_o \varepsilon_r \Delta x \Delta y}{T_d}$ farads.

The voltage developed across the resistive section in the z direction can be derived by observing

$$\Delta V(x,y,\omega_a) = I_{av}(\omega_a) R_{Tz} \quad \text{volts}$$

where $R_{Tz} = \frac{K T_p^2}{\Delta x \Delta y}$ ohms and $I_{av}(\omega_a)$ is the average current flowing in the z direction through the resistive section but

such that

$$I_{av}\ (\omega_a) < I_T\ (\omega_a) \text{ amperes}$$

Therefore

$$\Delta V(x,y,\omega_a) < \frac{I_T(\omega_a) K\ T_p^2}{\Delta x \Delta y} \text{ volts} \qquad .....4.3$$

The error quantity now becomes

$$\frac{\Delta V(x,y,\omega_a)}{V_c(x,y,\omega_a)} < \frac{j\omega_a \varepsilon_o \varepsilon_r\ K\ T_p^2}{T_d} \qquad .....4.4$$

Typical values for the variables are:

$$\omega_{a_{max}} \approx 7 \times 10^5 \text{ radians/sec}$$

$$\varepsilon_r \approx 4$$

$$K \approx 10^4 \text{ ohms/square}$$

$$T_p \approx 8 \times 10^{-5} \text{ metre}$$

$$T_d \approx 5 \times 10^{-5} \text{ metre}$$

On substitution,

$$\left|\frac{\Delta V(x,y,\omega_a)}{V_c(x,y,\omega_a)}\right| \underset{\text{typically}}{<} 3 \times 10^{-5} \qquad .....4.5$$

This shows that the voltage drop $\Delta V(x,y,\omega_a)$ even at high map frequencies is negligible compared with $V_c(x,y,\omega_a)$. The currents flowing in the plane of the paper, therefore, are not a function of the z-direction; that is

$I_i(x,z,t) = I_i(x,t)$ and $I_i(y,z,t) = I_i(y,t)$ amperes.

The elemental equivalent circuit of Figure 4:2 now applies. The voltages and currents are represented in the time domain. The directional resistances per unit length are

$$R'_x = \frac{\rho}{T_p \Delta y} = \frac{K}{\Delta y} \qquad \text{ohm/metre}$$

and $$R'_y = \frac{\rho}{T_p \Delta x} = \frac{K}{\Delta x} \qquad \text{ohm/metre}$$

4.3 The General Equations of the Map

Consider the voltages and currents in the equivalent circuit. From Kirchoff's voltage law one can write the following equations

$$V_c(x,y,t) = I(x+\Delta x,t)R'_x \Delta x + V_c(x+\Delta x,y,t) \text{ volts} \quad .....4.6$$

$$V_c(x,y,t) = I(y+\Delta y,t)R'_y \Delta y + V_c(x,y+\Delta y,t) \text{ volts} \quad .....4.7$$

Kirchoff's current law gives

$$I(x,t) = \lambda C \frac{\partial V_c(x,y,t)}{\partial t} + I(x+\Delta x,t)$$

$$= \lambda \frac{\varepsilon_o \varepsilon_r \Delta x \Delta y}{T_d} \frac{\partial V_c(x,y,t)}{\partial t} + I(x+\Delta x,t) \quad ....4.8$$

and

$$I(y,t) = (1-\lambda) C \frac{\partial V_c(x,y,t)}{\partial t} + I(y+\Delta y,t)$$

$$= (1-\lambda) \frac{\varepsilon_o \varepsilon_r \Delta x \Delta y}{T_d} \frac{\partial V_c(x,y,t)}{\partial t} + I(y+\Delta y,t)$$

$$.....4.9$$

The variable λ describes what fraction the quantity

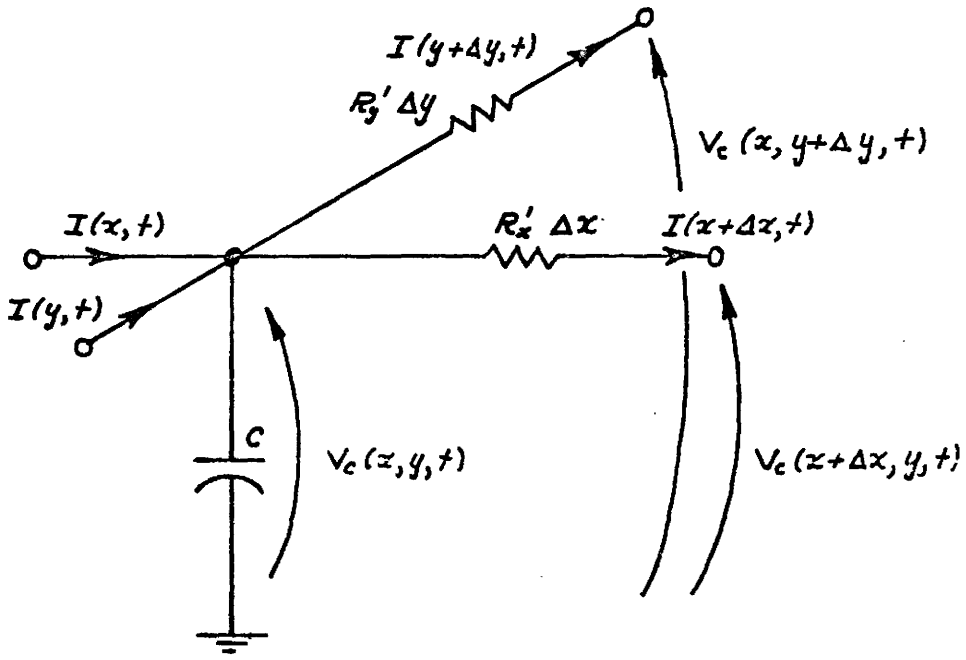

FIGURE 4.2 THE SIMPLIFIED EQUIVALENT CIRCUIT

$I(x,t) - I(x+\Delta x,t)$ represents of the total current flowing through the elemental equivalent capacitance C. The total current at any time t flowing through this capacitance is

$$C \frac{\partial V_c(x,y,t)}{\partial t} = \lambda C \frac{\partial V_c(x,y,t)}{\partial t} + (1 - \lambda) C \frac{\partial V_c(x,y,t)}{\partial t}$$

where λ is such that $0 \leq \lambda \leq 1$.

Rearranging the four equations 4:6, 4:7, 4:8 and 4:9 and taking limits as $\Delta x \to 0$ and $\Delta y \to 0$, one has

$$\lim_{\Delta x \to 0} \frac{V_c(x+\Delta x,y,t) - V_c(x,y,t)}{\Delta x} = \frac{\partial V_c(x,y,t)}{\partial x} = -I(x,t)R'_x$$

$$\lim_{\Delta y \to 0} \frac{V_c(x,y+\Delta y,t) - V_c(x,y,t)}{\Delta y} = \frac{\partial V_c(x,y,t)}{\partial y} = -I(y,t)R'_y$$

$$\lim_{\Delta x \to 0} \frac{I(x+\Delta x,t) - I(x,t)}{\Delta x} = \frac{\partial I(x,t)}{\partial x} = -\lambda \frac{\varepsilon_o \varepsilon_r \Delta y}{T_d} \frac{\partial V_c(x,y,t)}{\partial t}$$

$$\lim_{\Delta y \to 0} \frac{I(y+\Delta y,t) - I(y,t)}{\Delta y} = \frac{\partial I(y,t)}{\partial y} = -(1-\lambda) \frac{\varepsilon_o \varepsilon_r \Delta x}{T_d} \frac{\partial V_c(x,y,t)}{\partial t}$$

From the first two limit equations there results

$$I(x,t) = \frac{-1}{R'_x} \frac{\partial V_c(x,y,t)}{\partial x} \text{ and } I(y,t) = \frac{-1}{R'_y} \frac{\partial V_c(x,y,t)}{\partial y}$$

Substitution of the above two equations into the last two limit equations gives

$$\frac{\partial^2 V_c(x,y,t)}{\partial x^2} - \lambda R'_x \frac{\varepsilon_o \varepsilon_r \Delta y}{T_d} \frac{\partial V_c(x,y,t)}{\partial t} = 0$$

and

$$\frac{\partial^2 V_c(x,y,t)}{\partial y^2} - (1-\lambda)\, R'_y \frac{\varepsilon_o \varepsilon_r \Delta x}{T_d} \frac{\partial V_c(x,y,t)}{\partial t} = 0$$

Substituting for R'_x and R'_y, one obtains

$$\frac{\partial^2 V_c(x,y,t)}{\partial x^2} - \lambda \frac{K\, \varepsilon_o \varepsilon_r}{T_d} \frac{\partial V_c(x,y,t)}{\partial t} = 0$$

and

$$\frac{\partial^2 V_c(x,y,t)}{\partial y^2} - (1-\lambda) \frac{K\, \varepsilon_o \varepsilon_r}{T_d} \frac{\partial V_c(x,y,t)}{\partial t} = 0$$

Addition of the above two equations gives

$$\frac{\partial^2 V_c(x,y,t)}{\partial x^2} + \frac{\partial^2 V_c(x,y,t)}{\partial y^2} - \frac{K\, \varepsilon_o \varepsilon_r}{T_d} \frac{\partial V_c(x,y,t)}{\partial t} = 0 \qquad .....4.10$$

When the voltage is assumed to be sinusoidal, one can write $V_c(x,y,t)$ in its most general form as

$$V_c(x,y,t) = V_c(x,y,\omega_a)\, e^{j\omega_a t}$$

where

$$V_c(x,y,\omega_a) = |V_c(x,y,\omega_a)| e^{j\theta_c(x,y,\omega_a)}$$

Here $|V_c(x,y,\omega_a)|$ is the amplitude distribution and $\theta_c(x,y,\omega_a)$ is the phase distribution of $V_c(x,y,t)$.

Equation 4:10 may be written in terms of the capacitive current density $J_c(x,y,t)$ by observing that for an elemental section in the frequency domain one can write

$$V_c(x,y,\omega_a) = [J_c(x,y,\omega_a)\ \Delta x\Delta y]X_c = \frac{J_c(x,y,\omega_a)}{[j\omega_a \frac{\varepsilon_o\varepsilon_r}{T_d}]}$$

Therefore

$$V_c(x,y,t) = \frac{J_c(x,y,\omega_a)\ e^{j\omega_a t}}{[j\omega_a \frac{\varepsilon_o\varepsilon_r}{T_d}]} \qquad .....4.11$$

Substitution of equation 4.11 into 4.10 yields

$$\frac{\partial^2 J_c(x,y,\omega_a)}{\partial x^2} + \frac{\partial^2 J_c(x,y,\omega_a)}{\partial y^2} - j\omega_a \frac{K\ \varepsilon_o\varepsilon_r}{T_d} J_c(x,y,\omega_a) = 0$$

or

$$\nabla^2 J_c(x,y,\omega_a) - j\omega_a \frac{K\ \varepsilon_o\varepsilon_r}{T_d} J_c(x,y,\omega_a) = 0 \qquad .....4.12$$

This Helmholtz type equation has the same form as the differential equation governing the two-dimensional current density distribution $J_z(x,y,\omega)$ in a good conductor. The conductor is assumed to be in free space and sinusoidally excited. The derivation of this equation

$$\nabla^2 J_z(x,y,\omega) - j\omega\ \mu_o\mu_r\sigma\ J_z(x,y,\omega) = 0 \qquad .....4.13$$

is given in Appendix D.

Generally, it is impractical to create an analogue the same size as the real conductor as the use of the same co-ordinates in equations 4.12 and 4.13 imply. An analogue map is constructed so that it has the same proportional

geometry as that of the real conductor but usually on a different scale. Generally then, a scale factor k_o is assumed between the map and the real conductor dimensions. If the co-ordinates of a given map are x_m and y_m then

$$x_m = k_o\, x \quad \text{and} \quad y_m = k_o\, y$$

The governing equation in terms of the map co-ordinates is therefore

$$\nabla_m^2 J_c(x_m,y_m,\omega_m) - j\omega_m\, K\, \frac{\varepsilon_o \varepsilon_r}{T_d}\, J_c(x_m,y_m,\omega_m) = 0 \qquad .....4.14$$

where ∇_m^2 is the Laplacian in the map co-ordinates. If this co-ordinate system is changed to that in equation 4.12 and 4.13, one has

$$\frac{\partial^2}{\partial x_m^2} = \frac{1}{k_o^2}\, \frac{\partial^2}{\partial x^2} \quad \text{and} \quad \frac{\partial^2}{\partial y_m^2} = \frac{1}{k_o}\, \frac{\partial^2}{\partial y^2}$$

Then equation 4.14 becomes

$$\nabla^2 J_c(x,y,\omega_a) - j[k_o^2\, \omega_m]\, K\, \frac{\varepsilon_o \varepsilon_r}{T_d}\, J_c(x,y,\omega_a) = 0 \qquad ...4.15$$

The current density distributions $J_c(x_m,y_m,\omega_m)$ and $J_c(x,y,\omega_a)$ will be exactly the same when

$$\omega_a = k_o^2\, \omega_m \qquad .....4.16$$

At a certain angular frequency $\omega_a = k_1^2 \omega$ the relationship between the capacitive current density and the real conductor

density is given by

$$J_c(x,y,\omega_a) = k_2\ J_z(x,y,\omega) \qquad .....4.17$$

where the constant k_2 scales the current.

Also

$$J_c(x_m,y_m,\omega_m) = k_3\ J_z(x,y,\omega) \qquad .....4.18$$

where k_3 also scales the current.

The amplitude and phase distributions are therefore given by

$$|J_c(x_m,y_m,\omega_m)| = k_3\ |J_z(x,y,\omega)| \qquad .....4.19$$

and

$$\beta_c(x_m,y_m,\omega_m) = \alpha_z(x,y,\omega) \qquad .....4.20$$

Substitution of equation 4.17 into 4.15 gives

$$\nabla^2 J_z(x,y,\omega) - j[k_o^2\ \omega_m]^{K}\ \frac{\varepsilon_o\varepsilon_r}{T_d}\ J_z(x,y,\omega) = 0 \qquad .....4.21$$

Comparing equations 4.13 and 4.21 one has, therefore,

$$k_o^2\ \omega_m\ \frac{K\ \varepsilon_o\varepsilon_r}{T_d} = \omega\ \mu_o\mu_r\ \sigma \qquad .....4.22$$

The analogue map frequency is given in terms of the real frequency by

$$f_m = \frac{T_d\ \mu_o\mu_r\ \sigma}{k_o^2\ K\ \varepsilon_o\varepsilon_r}\ f \quad \text{Hz} \qquad .....4.23$$

The equation relating the surface voltage distribution $V(x,y,\omega_a)$ to the capacitive current density distribution $J_c(x,y,\omega_a)$ can be derived from the equivalent circuit shown in Figure 18.

Kirchoff's current law applied to the node gives

$$I(x,t) + I(y,t) + J_c(x,y,t)\,\Delta x\Delta y = I(x+\Delta x,t) + I(y+\Delta y,t) \qquad .....4.24$$

where

$$I(x,t) = J(x,t)\,\Delta y\,T_p$$

$$I(y,t) = J(y,t)\,\Delta x\,T_p$$

$$I(x+\Delta x,t) = \left[J(x,t) + \frac{\partial J(x,t)}{\partial x}\,\Delta x\right]\Delta y\,T_p$$

$$I(y+\Delta y,t) = \left[J(y,t) + \frac{\partial J(y,t)}{\partial y}\,\Delta y\right]\Delta x\,T_p$$

Thus

$$\frac{\partial J(x,t)}{\partial x} + \frac{\partial J(y,t)}{\partial y} = \frac{J_c(x,y,t)}{T_p} \qquad .....4.25$$

From Ohm's law one has for $\Delta x \to 0$ and $\Delta y \to 0$

$$E(x,t) = \frac{\partial V(x,y,t)}{\partial x} = -\rho_x\,J(x,t)$$

and

$$E(y,t) = \frac{\partial V(x,y,t)}{\partial y} = -\rho_y\,J(y,t)$$

For $\rho_x = \rho_y = \rho$

$$J(x,t) = -\frac{1}{\rho}\frac{\partial V(x,y,t)}{\partial x} \qquad .....4.26$$

and

$$J(y,t) = -\frac{1}{\rho}\frac{\partial V(x,y,t)}{\partial y} \qquad .....4.27$$

Substitution of equations 4.26 and 4.27 into 4.25 yield

$$\frac{\partial^2 V(x,y,t)}{\partial x^2} + \frac{\partial^2 V(x,y,t)}{\partial y^2} = \frac{-\rho}{T_p} J_c(x,y,t)$$

or

$$\nabla^2 V(x,y,t) = -K J_c(x,y,t) \qquad .....4.28$$

If equation 4.28 is written in terms of the map coordinates used in equation 4.14, one has

$$\nabla_m^2 V(x_m,y_m,t) = -K J_c(x_m,y_m,t) \qquad .....4.29$$

For

$$V(x_m,y_m,t) = V(x_m,y_m,\omega_m)\, e^{j\omega_m t}$$

where

$$V(x_m,y_m,\omega_m) = |V(x_m,y_m,\omega_m)| e^{j\psi(x_m,y_m,\omega_m)}$$

and

$$J_c(x_m,y_m,t) = J_c(x_m,y_m,\omega_m)\, e^{j\omega_m t}$$

where

$$J_c(x_m,y_m,\omega_m) = |J_c(x_m,y_m,\omega_m)|\, e^{j\beta_c(x_m,y_m,\omega_m)}$$

equation 4.29 becomes

$$\nabla_m^2 V(x_m,y_m,\omega_m) = - K\, J_c(x_m,y_m,\omega_m) \qquad .....4.30$$

This equation has the same form as the differential equation governing the magnetic vector potential in two dimensions as derived in Appendix A. Thus, the surface voltage distribution $V(x_m,y_m,\omega_m)$ is directly analogous to the magnetic vector potential $A_z(x,y,\omega)$ and the capacitive current density distribution $J_c(x_m,y_m,\omega_m)$ is directly analogous to the conductor current density distribution $J_z(x,y,\omega)$.

Therefore, at that frequency f_m which makes

$$J_c(x_m,y_m,\omega_m) = k_3\, J_z(x,y,\omega)$$

one has the result

$$V(x_m,y_m,\omega_m) = k_4\, A_z(x,y,\omega)$$

where

$$k_4 = \left(\frac{K}{\mu_o \mu_r}\right) k_3$$

Therefore

$$|V(x_m,y_m,\omega_m)| = k_4\, |A_z(x,y,\omega)|$$

and

$$\psi(x_m,y_m,\omega_m) = \phi(x,y,\omega)$$

CHAPTER 5

5.1 Introduction

The equations developed in Chapter 4 indicate that a possible analogue for a conductor carrying current at any frequency is theoretically possible. The three important equations are

(i) $$\nabla_m^2 J_c(x_m,y_m,\omega_m) - j\omega_m \frac{K\ \varepsilon_o\varepsilon_r}{T_d} J_c(x_m,y_m,\omega_m) = 0$$

(ii) $$\nabla_m^2 V(x_m,y_m,\omega_m) = - K\ J_c(x_m,y_m,\omega_m)$$

(iii) $$f_m = \frac{T_d\ \mu_o\mu_r\ \sigma}{k_o^2\ K\ \varepsilon_o\varepsilon_r} f \qquad H_z$$

The last equation shows that the analogue frequency f_m can be obtained directly in terms of the parameters of the analogue and real systems when the scale factor k_o is known. At this analogue frequency f_m, the current density distribution is the same as that in the real conductor. The surface voltage distribution is directly analogous to the magnetic vector potential. The analogy may be demonstrated experimentally if the magnetic vector potential in a circular conductor can be calculated.

5.2 Magnetic Vector Potential for a Circular Conductor

Consider the current density distribution in a circular conductor. As shown in Appendix E, the current

density distribution in the frequency domain is given by

$$J_z(r,\omega) = J_s \frac{J_o(\tau r)}{J_o(\tau r_o)} \qquad \text{amps/m}^2 \qquad .....5.1$$

where

$$\tau = j^{-\frac{1}{2}} [\omega \mu_o \mu_r \sigma]^{\frac{1}{2}}$$

and r_o is the radius of the circular conductor
and J_s is the surface current density
and $J_o(\tau r)$ is a zero order Bessel function of the first kind with a complex argument.

The magnetic field density in the sinusoid steady state can be obtained from Faraday's law written as

$$\nabla x\, E_z(r,\omega) = - j\omega\, B_\phi(r,\omega) \qquad .....5.2$$

Since the cylindrical co-ordinate system has been used only r-derivates remain

Thus $$B_\phi(r,\omega) = \frac{1}{j\omega} \frac{dE_z(r,\omega)}{dr} \qquad .....5.3$$

From Ohm's law, one has

$$E_z(r,\omega) = \frac{1}{\sigma} J_z(r,\omega)$$

Therefore

$$B_\phi(r,\omega) = \frac{-j}{\omega\sigma} \frac{dJ_z(r,\omega)}{dr} \qquad .....5.4$$

The magnetic flux density is also given in terms

of the magnetic vector potential $A_z(r,\omega)$ as

$$B_\phi(r,\omega) = \nabla \times A_z(r,\omega)$$

or

$$B_\phi(r,\omega) = -\frac{dA_z(r,\omega)}{dr} \qquad .....5.5$$

Therefore

$$\frac{dA_z(r,\omega)}{dr} = \frac{j}{\omega\sigma}\frac{dJ_z(r,\omega)}{dr}$$

Integrating both sides and adding an integration constant A_o, one has

$$A_z(r,\omega) = \frac{j}{\omega\sigma} J_z(r,\omega) + A_o \qquad .....5.6$$

Substitution for $J_z(r,\omega)$ gives

$$A_z(r,\omega) = \frac{jJ_s}{\omega\sigma}\frac{J_o(\tau r)}{J_o(\tau r_o)} + A_o \qquad .....5.7$$

For convenience, one can choose the integration constant A_o such that the magnetic vector potential $A_z(r,\omega)$ is zero at $r = r_o$.

Therefore

$$A_o = \frac{-jJ_s}{\omega\sigma}$$

and thus the magnetic vector potential is

$$A_z(r,\omega) = \frac{jJ_s}{\omega\sigma}\left[\frac{J_o(\tau r) - J_o(\tau r_o)}{J_o(\tau r_o)}\right] \qquad .....5.8$$

The Bessel function $J_o(\tau r)$ can be written in terms of magnitude and phase angle as

$$J_o(\tau r) = M_o(\tau r)\, e^{j\beta_o(\tau r)}$$

Thus, equation 5.8 can be written as

$$A_z(r,\omega) = \frac{jJ_s}{\omega\sigma}\left[\frac{M_o(\tau r)}{M_o(\tau r_o)}\, e^{j[\beta_o(\tau r) - \beta_o(\tau r_o)]} - 1.0\right] \qquad .....5.9$$

The instantaneous value of the magnetic vector potential is given by the magnitude of equation 5.9.

The magnetic vector potential for the zero frequency case can be calculated from equation 5.8. The series expansion for the Bessel function $J_o(\tau r)$ can be expressed as

$$J_o(\tau r) = 1 - (\tau r/2)^2 + \frac{(\tau r/2)^4}{4} \ldots.$$

Thus equation 5.8 becomes

$$A_z(r,\omega) = \frac{jJ_s}{\omega\sigma}\left[\frac{(\tau r_o/2)^2 - (\tau r/2)^2 + \frac{(\tau r_o/2)^4}{4} - \frac{(\tau r/2)^4}{4} \ldots.}{1 - (\tau r_o/2)^2 + \frac{(\tau r_o/2)^4}{4} \ldots.}\right]$$

Since

$$\tau^2 = -j\omega\mu\sigma$$

Then

$$A_z(r,\omega) = \frac{jJ_s}{\omega\sigma}\left[\frac{\frac{-j\omega\mu\sigma r_o^2}{4} + \frac{j\omega\mu\sigma r^2}{4} - \frac{\omega^2\mu^2\sigma^2 r_o^4}{64} + \frac{\omega^2\mu^2\sigma^2 r^4}{64} \ldots.}{1 - \frac{j\omega\mu\sigma r_o^2}{4} - \frac{\omega^2\mu^2\sigma^2 r_o^4}{64} \ldots\ldots}\right]$$

Therefore

$$\lim_{\omega \to 0} A_z(r,\omega) = jJ_s \left[\frac{-j\mu r_o^2}{4} + \frac{j\mu r^2}{4}\right] = \frac{\mu J_s}{4} [r_o^2 - r^2]$$

At $\omega = 0$, $J_s = J_{dc}$

Thus

$$A_z(r) = \frac{\mu J_{dc}}{4} [r_o^2 - r^2] \quad \text{webers/m} \quad .....5.10$$

The maximum value of the magnetic vector potential is given when $r = 0$ because of the choice of the integration constant A_o. Therefore

$$A_{z_{max}}(r) = A_z(o) = \frac{\mu J_{dc}}{4} r_o^2 \quad \text{webers/m} \quad .....5.11$$

The total flux per unit length between the centre and the surface of the conductor is given by

$$\phi_T' = \int_o^{r_o} B_\phi(r)\, dr \qquad .....5.12$$

where

$$B_\phi(r) = \mu H_\phi(r) = \frac{\mu I}{2\pi r_o^2} r = \frac{\mu J_{dc}}{2} r \qquad .....5.13$$

Therefore

$$\phi_T' = \frac{\mu J_{dc}}{4} r_o^2 \qquad \text{webers/m}$$

The total flux per unit length is equivalent to the value of the magnetic vector potential at $r = 0$. The flux per unit length contained between any two points a and b between $r = 0$ and $r = r_o$ is given by

$$\phi'_{ab} = |A_z(r_a)-A_z(r_b)| \qquad \text{webers/m} \qquad .....5.14$$

5.3 Flux Density Distribution for a Circular Conductor

An expression for the magnetic flux density at any angular frequency ω can be derived. From equation 5.4 one has

$$B_\phi(r,\omega) = \frac{-j}{\omega\sigma}\frac{dJ_z(r,\omega)}{dr}$$

or

$$B_\phi(r,\omega) = \frac{-j\tau J_s}{\omega\sigma\, J_o(\tau r_o)}\frac{dJ_o(\tau r)}{d(\tau r)}$$

A property of the Bessel functions $J_o(\tau r)$ and $J_1(\tau r)$ is that

$$\frac{dJ_o(\tau r)}{d(\tau r)} = -J_1(\tau r)$$

Therefore

$$B_\phi(r,\omega) = \frac{j\tau J_s}{\omega\sigma}\frac{J_1(\tau r)}{J_o(\tau r_o)}$$

Since

$$\tau = j^{-\frac{1}{2}}[\omega\mu\sigma]^{\frac{1}{2}}$$

Thus

$$B_\phi(r,\omega) = j^{\frac{1}{2}}\left[\frac{\mu}{\omega\sigma}\right]^{\frac{1}{2}} J_s\frac{J_1(\tau r)}{J_o(\tau r_o)} \qquad .....5.15$$

When the magnitude and phase angle representation of the Bessel functions $J_o(\tau r)$ and $J_1(\tau r)$ are substituted in

equation 5.15, one has

$$B_\phi(r,\omega) = j^{\frac{1}{2}} \left[\frac{\mu}{\omega\sigma}\right]^{\frac{1}{2}} J_s \frac{M_1(\tau r)}{M_o(\tau r_o)} e^{j[\beta_1(\tau r)-\beta_o(\tau r_o)]} \qquad .....5.16$$

The instantaneous value of the magnetic flux density is given by the magnitude of equation 5.16.

The flux density for the zero frequency case can be obtained from equation 5.15. The series expansion for the Bessel function $J_1(\tau r)$ is

$$J_1(\tau r) = (\tau r/2) - \frac{(\tau r/2)^3}{2} + \frac{(\tau r/2)^5}{12}.....$$

$$= (\tau r/2)\left[1 - \frac{(\tau r/2)^2}{2} + \frac{(\tau r/2)^4}{12} \cdots\right]$$

Thus equation 5.15 becomes

$$B_\phi(r,\omega) = j^{\frac{1}{2}} \left[\frac{\mu}{\omega\sigma}\right]^{\frac{1}{2}} J_s \left(\frac{\tau r}{2}\right) \left[\frac{1-\frac{(\tau r/2)^2}{2} + \frac{(\tau r/2)^4}{12}....}{1-(\tau r_o/2)^2 + \frac{(\tau r_o/2)^4}{4}...}\right]$$

or

$$B_\phi(r,\omega) = \frac{\mu J_s r}{2}\left[\frac{1+\frac{j\omega\mu\sigma r^2}{8} - \frac{j\omega^2\mu^2\sigma^2 r^4}{192}....}{1+\frac{j\omega\mu\sigma r_o^2}{4} - \frac{\omega^2\mu^2\sigma^2 r_o^4}{64}...}\right]$$

Therefore

$$\lim_{\omega\to o} B_\phi(r,\omega) = \frac{\mu J_s}{2} r$$

or

$$B_\phi(r) = \frac{\mu J_{dc}}{2} r \qquad \text{teslas}$$

5.4 Experimental Validation

An analogue map for the circular conductor was constructed as shown in Figure 5:1. The dc capacitance of the map is given by

$$C_{dc} = \frac{\varepsilon_o \varepsilon_r}{T_d} \times \text{Area} \qquad \text{F}$$

or

$$C_{dc} = \frac{\varepsilon_o \varepsilon_r \pi \ r_m^2 \ \theta}{360 \ T_d} \qquad \text{F} \qquad \text{.....5.17}$$

The shunt capacitance of the map was measured using the circuit shown in Figure 5:1. The source frequency f_s is low enough such that

$$C_s(f_s) = C_{dc}$$

For the constructed map it was found that

$$C_{dc} = 0.0181 \ \mu\text{F}$$
$$r_m = 25.3 \ \text{cm}$$
$$\theta = 33.5^\circ$$

Therefore

$$\frac{T_d}{\varepsilon_o \varepsilon_r} = 1.04 \times 10^6$$

The resistance per square of the paper was found to be

$$K = 9.9 \ \text{K}\Omega/\text{square}$$

If the conductor in the real system is chosen to be

MEASUREMENT OF THE SURFACE VOLTAGE DISTRIBUTION

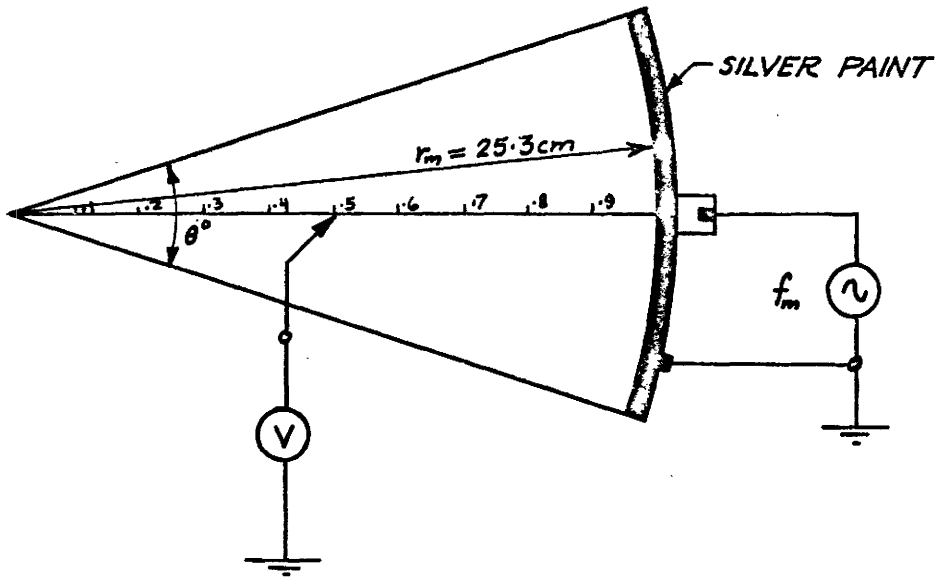

MEASUREMENT OF THE SHUNT CAPACITANCE C_s OF THE MAP

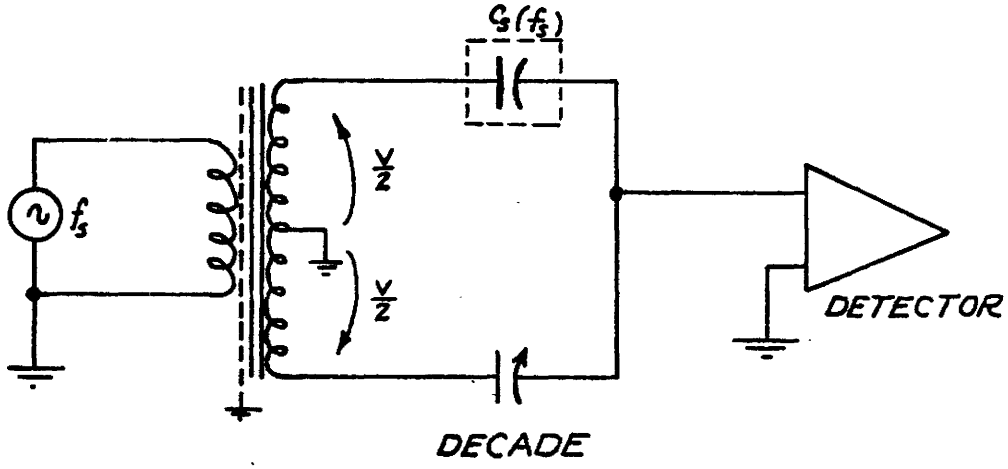

f_s SUCH THAT $C_s(f_s) = C_{dc}$

FIGURE 5.1 ANALOGUE FOR THE CIRCULAR CONDUCTOR

a copper wire with a radius of 0.1 cm, one has

$$\sigma_{cu} = 5.8 \times 10^7 \quad \text{mhos/metre}$$

$$\mu_r = 1.0$$

and the scale factor is

$$k_o = \frac{r_m}{r_o} = 25.3$$

The map frequency given by equation 4.23 becomes

$$f_m = 12f \quad H_z$$

The normalized instantaneous distribution of the magnetic vector potential as a function of radius was calculated from equation 5.8. Distributions were calculated for $[\omega\mu_o\sigma]^{\frac{1}{2}} r_o = 2$, 4, 8, and 10. The corresponding frequencies are 87.5 (base frequency), 350, 1400, and 2188 Hz. These distributions are plotted in Figure 5:2.

The equivalent map base frequency should have been

$$f_m = 12 \times 87.5 = 1050 \ H_z$$

In fact, the normalized surface voltage distributions which had the best fit to the theoretical distributions had a base frequency of about 1100 Hz. The approximate experimental error in the calculation of the true analogue frequency was 5%.

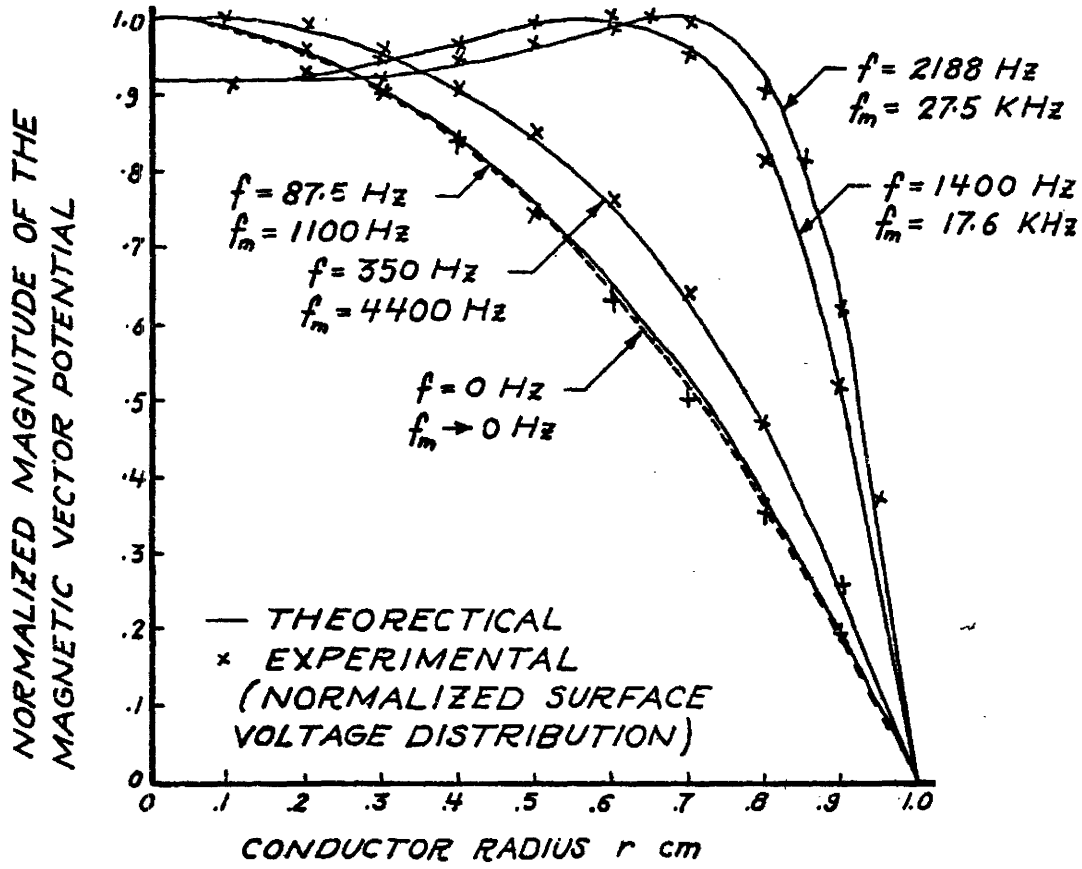

FIGURE 5.2 DISTRIBUTIONS OF THE MAGNITUDE OF THE MAGNETIC VECTOR POTENTIAL AT DIFFERENT FREQUENCIES

5.5 Conclusions

This thesis has described an improved capacitively-coupled multiple-source analogue system using conducting paper.

An improved analogue map construction technique has been demonstrated. A thin tape dielectric is used instead of a glass dielectric. A method of connection to the silver-painted capacitively-coupled electrodes has been developed which allows the creation of a physically flat map. Construction time for a typical multiple source map is about two hours.

The analogue allows equipotentials which represent lines of constant magnetic vector potential (flux lines) to be plotted. An efficient null technique has been devised to locate the equipotentials on the map surface in percentage values. The heart of this technique is that one of the kernel points (points of zero flux density in the magnetic system) is brought to virtual ground potential via a Wagner Earth circuit.

Analogous values of flux density are obtained in terms of differential voltages on the conducting paper surface. These voltages are conveniently measured using a double probe and a FET-inputed differential amplifier.

The accuracy of the system is good. Flux line and

flux density accuracy have been defined in terms of the magnetic field of a circular conductor carrying dc in free space. Flux lines or lines of constant magnetic vector potential can be located to within approximately ± 1%. Flux density information can be obtained with approximately ± 3% error.

A generalized theory of the capacitively-coupled analogue is given. The thickness of the conducting paper is shown to have negligible influence on the accuracy of the surface voltage distribution for typical parameters of the system. The equation governing the capacitive current distribution as a function of frequency is derived. This equation has the same form as the equation describing the current density distribution in a real conductor. The equation relating the surface voltage distribution at any frequency in terms of the capacitive current density distribution is derived. This equation has the same form as the differential equation relating the magnetic vector potential to the conductor current density distribution. The equation relating the map frequency and the real frequency in terms of the parameters of the analogue and real systems is derived. At this analogue frequency, the capacitive current density distribution is the same as the real conductor current density distribution.

The distribution at any frequency of the magnetic

vector potential and flux density as a function of radius in a circular conductor in free space is derived. The variation of the surface voltage distribution (analogous to the magnetic vector potential distribution) at different map frequencies for the analogue equivalent of a circular conductor was obtained. The actual map frequencies which gave the best agreement with the calculated magnetic vector potential distributions were about 5% in error. The error is probably attributable to:-

(i) inhomogeneity of the dielectric

(ii) inhomogeneity of the conducting paper

(iii) map loading due to shunt capacitance of the measuring probe.

Although the analogue has been described in terms of representing the magnetic system, other two-dimensional systems in engineering and science may be simulated. The sole criterion is that they have a common basis of interchangeable mathematics.

5.6 Scope of Future Work

(i) The experimental error found in the predicted map frequency, i.e.

$$f_m = \frac{T_d \mu_o \mu_r \sigma}{k_o^2 K \varepsilon_o \varepsilon_r} f \quad \text{Hz}$$

and the actual map frequency that must be used to give

a certain current density distribution in the real conductor must be investigated. It is hoped that this error could be reduced below 1%.

(ii) The need to simulate regions of different relative permeability is sometimes useful. The problem, therefore, is to create within a prescribed region of the conducting paper a uniform resistance per square K_r such that

$$K_r = \mu_r K \qquad \text{ohms/square}$$

That is, within the given region the resistivity of the paper must be raised by a factor μ_r over that outside the region. Alternatively, the resistivity outside the region must be lowered by a factor μ_r.

(iii) The new skin effect analogue outlined in Chapters 4 and 5 implies a more general analogue. This general analogue system would have capacitively-coupled multiple sources. Each source would have controllable magnitude and phase with respect to each other at any frequency.

A special case of this analogue would have all the sources controllable in magnitude and phase but at a single frequency. (Both proposed analogues are shown in Figure 5:3). In application, this analogue could map the instantaneous magnetic vector potential distribution of a system of conductors carrying three phase currents at mains supply frequency.

FREQUENCY, AMPLITUDE & PHASE VARIABLE

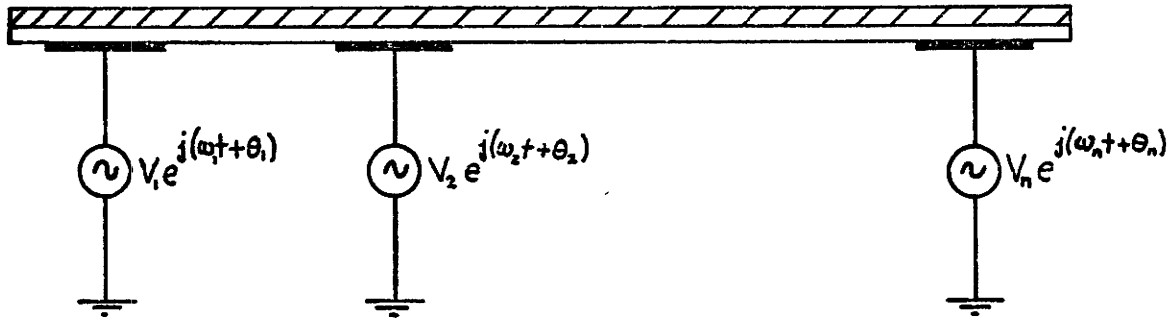

FREQUENCY FIXED, AMPLITUDE & PHASE VARIABLE

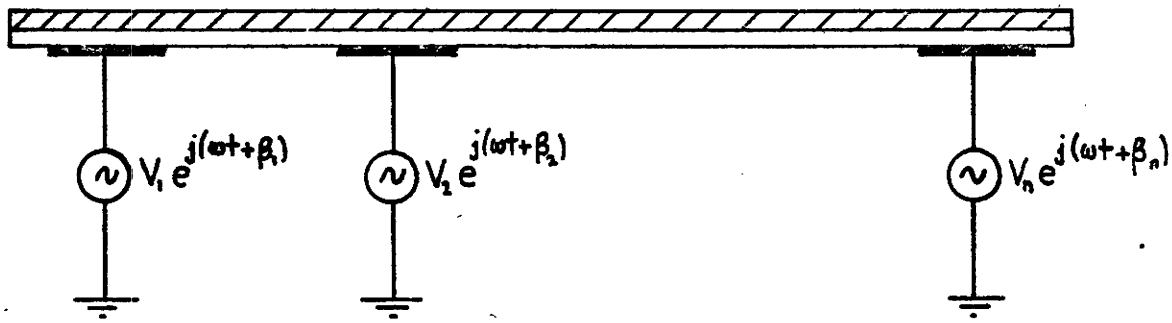

FIGURE 5.3 GENERAL CAPACITIVELY-COUPLED ANALOGUES

APPENDIX A

The Time Varying Two-Dimensional Magnetic Vector Potential

This derivation applies for homogeneous, isotropic materials.[10] A magnetic vector potential $A_z(x,y,t)$ is assumed such that the tangential flux density $B_t(x,y,t)$ can be derived from it by

$$B_t(x,y,t) = \nabla x\ A_z(x,y,t) \qquad A.1$$

Faraday's law is

$$\nabla x\ E_z(x,y,t) = -\frac{\partial B_t(x,y,t)}{\partial t} \qquad A.2$$

or on substitution

$$\nabla x\ [E_z(x,y,t) + \frac{\partial A_z(x,y,t)}{\partial t}\ ] = 0$$

This implies that the vector

$$E_z(x,y,t) + \frac{\partial A_z(x,y,t)}{\partial t}$$

may be derived as a gradient of a scalar Φ.

Therefore

$$E_z(x,y,t) + \frac{\partial A_z(x,y,t)}{\partial t} = -\nabla\Phi$$

or

$$E_z(x,y,t) = - \nabla\Phi - \frac{\partial A_z(x,y,t)}{\partial t} \qquad A.3$$

Another of Maxwell's equations states that

$$\nabla x\ H_t(x,y,t) = J_z(x,y,t) + \frac{\partial D_z(x,y,t)}{\partial t} \qquad A.4$$

where

$$H_t(x,y,t) = \frac{1}{\mu} B_t(x,y,t) \qquad A.5$$

and

$$D_z(x,y,t) = \varepsilon\ E_z(x,y,t) \qquad A.6$$

On substitution of equations A.3, A.5 and A.6 into A.4, one has

$$\frac{1}{\mu} \nabla x\ B_t(x,y,t) = J_z(x,y,t) + \varepsilon \frac{\partial}{\partial t} \left[-\nabla\Phi - \frac{\partial A_z(x,y,t)}{\partial t}\right]$$

or

$$\nabla x \nabla x\ A_z(x,y,t) = \mu J_z(x,y,t) + \mu\varepsilon \left[-\nabla\left(\frac{\partial \Phi}{\partial t}\right) - \frac{\partial^2 A_z(x,y,t)}{\partial t^2}\right] \qquad A.7$$

From vector calculus, one obtains the identity

$$\nabla x \nabla x\ A_z(x,y,t) = \nabla(\nabla \cdot A_z(x,y,t)) - \nabla^2 A_z(x,y,t)$$

Equation A.7 therefore becomes

$$\nabla(\nabla \cdot A_z(x,y,t)) - \nabla^2 A_z(x,y,t) = \mu J_z(x,y,t) - \mu\varepsilon \nabla\left(\frac{\partial \Phi}{\partial t}\right) - \mu\varepsilon \frac{\partial^2 A_z(x,y,t)}{\partial t^2} \qquad A.8$$

The Helmholtz theorem states that a vector is completely determined by specification of its divergence and its curl. Since the curl of $A_z(x,y,t)$ has been specified as $\nabla x\ A_z(x,y,t) = B_t(x,y,t)$ one is free to choose the divergence.

If the divergence of $A_z(x,y,t)$ is

$$\nabla \cdot A_z(x,y,t) = -\mu\varepsilon \frac{\partial \Phi}{\partial t} \quad \text{(Lorentz condition)} \qquad \text{A.9}$$

then equation A.8 becomes

$$\nabla^2 A_z(x,y,t) - \mu\varepsilon \frac{\partial^2 A_z(x,y,t)}{\partial t^2} = -\mu\ J_z(x,y,t) \qquad \text{A.10}$$

When the excitation is assumed to be sinusoidal, one can write

$$A_z(x,y,t) = A_z(x,y,\omega)\ e^{j\omega t} \qquad \text{A.11}$$

and

$$J_z(x,y,t) = J_z(x,y,\omega)\ e^{j\omega t} \qquad \text{A.12}$$

and

$$J_s(t) = |J_s(\omega)|\ e^{j\omega t}$$

where

$$A_z(x,y,\omega) = |A_z(x,y,\omega)|\ e^{j\phi(x,y,\omega)}$$

and

$$J_z(x,y,\omega) = |J_z(x,y,\omega)|\ e^{j\alpha(x,y,\omega)}$$

Here $|A_z(x,y,\omega)|$ and $\phi(x,y,\omega)$ describe the amplitude and phase distribution of the magnetic vector potential respectively. Also $|J_z(x,y,\omega)|$ and $\alpha(x,y,\omega)$ describe the amplitude

and phase distribution of the conductor current density. The phase of the surface current density $J_s(t)$ is taken as zero reference.

When equations A.11 and A.12 are substituted into A.10, one has

$$\nabla^2 A_z(x,y,\omega) + \omega^2 \mu\varepsilon\, A_z(x,y,\omega) = -\mu\, J_z(x,y,\omega) \quad \text{A.14}$$

For the case of a good conductor where the frequency f is below approximately 10^8 Hz, equation A.14 becomes

$$\nabla^2 A_z(x,y,\omega) = -\mu_o \mu_r\, J_z(x,y,\omega) \quad \text{A.15}$$

APPENDIX B

Constant Amplitude Phase Shifter[13]

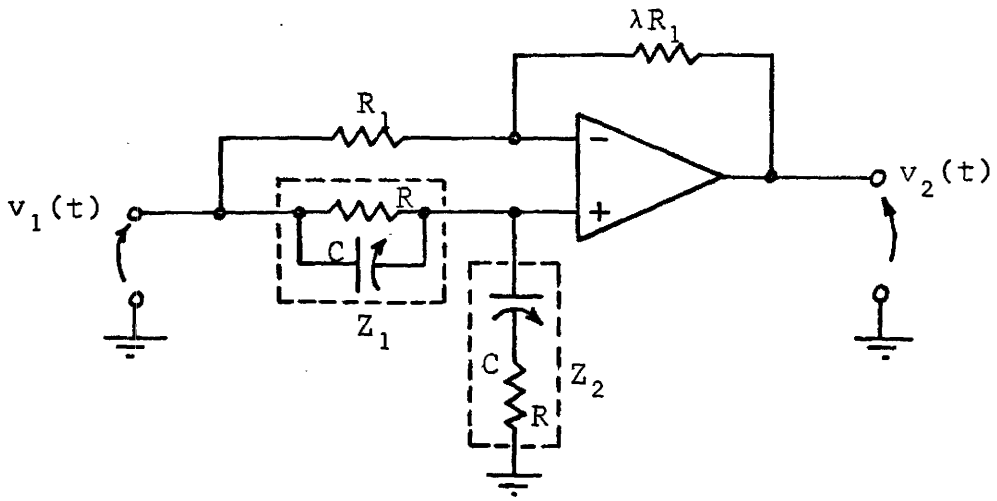

The output voltage $v_2(t)$ for the operational amplifier configuration shown is

$$v_2(t) = \frac{Z_2}{Z_1 + Z_2}(1 + \lambda)\ v_1(t) - \lambda\ v_1(t)$$

non-inverting | inverting

The transfer function can be written as

$$\frac{v_2(t)}{v_1(t)} = \frac{(1 + \lambda)}{[1 + \frac{1}{Z_1^{-1}\ Z_2}]} - \lambda$$

where $Z_1^{-1} = R^{-1} + j\omega C$ and $Z_2 = R + (j\omega C)^{-1}$

$$\frac{v_2(t)}{v_1(t)} = \frac{(1 + \lambda)}{[1 + \frac{1}{2+j(\omega RC-(\omega RC)^{-1})}]} - \lambda = \frac{(1+\lambda)[2+j(\omega RC-(\omega RC)^{-1}]}{3 + j(\omega RC-(\omega RC)^{-1})} - \lambda$$

or

$$\frac{v_2(t)}{v_1(t)} = \frac{2 - \lambda + j(\omega RC-(\omega RC)^{-1})}{3 + j\ (\omega RC-(\omega RC)^{-1})} = \frac{\frac{2-\lambda}{3} + j\ \frac{(\omega RC-(\omega RC)^{-1})}{3}}{3 + j\ \frac{(\omega RC-(\omega RC)^{-1})}{3}}$$

When $\lambda = 5$

$$\frac{v_2(t)}{v_1(t)} = - \frac{1 - j\frac{(\omega RC-(\omega RC)^{-1})}{3}}{1 + j\frac{(\omega RC-(\omega RC)^{-1})}{3}}$$

Therefore

$$\left|\frac{v_2(t)}{v_1(t)}\right| = 1$$

and the phase angle θ is given by

$$\theta = -2 \tan^{-1} \left[\frac{(\omega RC-(\omega RC)^{-1})}{3}\right] \text{ radians}$$

When $\omega RC \to 0$, $\theta \to 0°$

When $\omega RC \to 1$, $\theta \to + 180°$

When $\omega RC \to \infty$, $\theta \to 360°$

The circuit has been practically implemented in the form shown in Figure 2:4. The circuit will shift phase over 180° with less than 2% variation in voltage amplitude.

APPENDIX C

Derivation of Correction Factor for Anisotropic Conducting Paper

Considering the currents in the elemental paper section for Figure 1:5, one obtains equation 1.1, viz,

$$\frac{\partial J(x,t)}{\partial x} + \frac{\partial J(y,t)}{\partial y} = \frac{J_c(t)}{T_p} \qquad C.1$$

When the two directional resistivities of the conducting paper are considered, equations 1.2 and 1.3 become, respectively,

$$J(x,t) = \frac{-1}{\rho_x} \frac{\partial V(x,y,t)}{\partial x} \qquad C.2$$

and

$$J(y,t) = \frac{-1}{\rho_y} \frac{\partial V(x,y,t)}{\partial y} \qquad C.3$$

On substitution of C.2 and C.3 into C.1 there results

$$\frac{1}{\rho_x} \frac{\partial^2 V(x,y,t)}{\partial x^2} + \frac{1}{\rho_y} \frac{\partial^2 V(x,y,t)}{\partial y^2} = \frac{-J_c(t)}{T_p} \qquad C.4$$

When $\rho_x = \rho_y = \rho$, one has

$$\frac{\partial^2 V(x,y,t)}{\partial x^2} + \frac{\partial^2 V(x,y,t)}{\partial y^2} = \frac{-\rho}{T_p} J_c(t) \qquad C.5$$

If the x co-ordinate is altered by some factor $u = f(x)$ (such that $x = f^{-1}(u)$) in order to compensate for the difference between ρ_x and ρ_y, equation C.1 becomes

$$\frac{\partial J(u,t)}{\partial x}\left(\frac{\partial x}{\partial u}\right) + \frac{\partial J(y,t)}{\partial y} = \frac{J_c(t)}{T_p} \qquad C.6$$

Here

$$J(u,t) = \frac{-1}{\rho_u}\frac{\partial V(x,y,t)}{\partial u} \qquad C.7$$

Since $J(u,t) = J(x,t)$ one must have $\rho_u = \rho_x$

Then

$$J(u,t) = \frac{-1}{\rho_x}\frac{\partial V(x,y,t)}{\partial x}\left(\frac{\partial x}{\partial u}\right) \qquad C.8$$

Therefore

$$\frac{\partial J(u,t)}{\partial x} = -\frac{1}{\rho_x}\frac{\partial^2 V(x,y,t)}{\partial x^2}\left(\frac{\partial x}{\partial u}\right) - \frac{1}{\rho_x}\frac{\partial V(x,y,t)}{\partial x}\frac{\partial}{\partial x}\left(\frac{\partial x}{\partial u}\right) \qquad C.9$$

and

$$\frac{J(y,t)}{\partial y} = \frac{-1}{\rho_y}\frac{\partial^2 V(x,y,t)}{\partial y^2} \qquad C.10$$

Thus equation C.6 becomes

$$\frac{1}{\rho_x}\frac{\partial^2 V(x,y,t)}{\partial x^2}\left(\frac{\partial x}{\partial u}\right)^2 + \frac{1}{\rho_x}\frac{\partial V(x,y,t)}{\partial x}\left(\frac{\partial x}{\partial u}\right)\frac{\partial}{\partial x}\left(\frac{\partial x}{\partial u}\right) + \frac{1}{\rho_y}\frac{\partial^2 V(x,y,t)}{\partial y^2} = -\frac{J_c(t)}{T_p} \qquad C.11$$

If equation C.11 is to have the same form as C.5, one must have

$$\frac{1}{\rho_x} \frac{\partial V(x,y,t)}{\partial x} \left(\frac{\partial x}{\partial u}\right) \frac{\partial}{\partial x} \left(\frac{\partial x}{\partial u}\right) = 0$$

Since $\frac{\partial V(x,y,t)}{\partial x} \neq 0$ one can make $\frac{\partial}{\partial x} \left(\frac{\partial x}{\partial u}\right) = 0$ implying

$\frac{du}{dx}$ = a constant C.12

Also, one must have $\frac{1}{\rho_x} \left(\frac{\partial x}{\partial u}\right)^2 = \frac{1}{\rho_y}$ or $\frac{du}{dx} = \left(\frac{\rho_y}{\rho_x}\right)^{\frac{1}{2}}$

C.13

When $u = \left(\frac{\rho_y}{\rho_x}\right)^{\frac{1}{2}} x$, equations C.12 and C.13 are satisfied. That is, all the dimensions in the x direction are multiplied by a factor $\left(\frac{\rho_x}{\rho_y}\right)^{\frac{1}{2}}$.

APPENDIX D

The Differential Equation for Skin Effect

Consider the homogeneous, isotropic, conducting

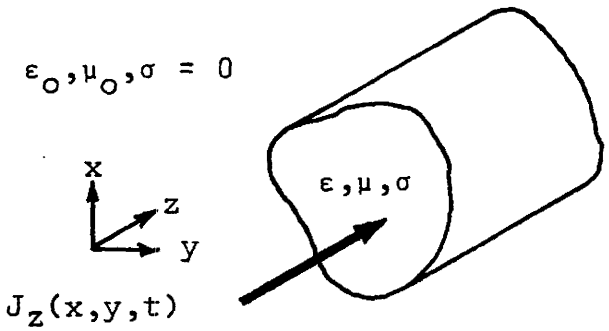

medium of arbitrary cross-section in free space shown above. The conducting medium is assumed to be sinusoidally excited at an angular frequency of ω radians/sec. Within the conducting medium, the electric field $E_z(x,y,t)$ and the tangential magnetic field intensity $H_t(x,y,t)$ are governed by Maxwell's equations. These equations are:

(a) $$\nabla \cdot E_z(x,y,t) = \frac{\rho(t)}{\varepsilon} = 0 \qquad \text{D.1}$$

The volume charge density $\rho(t)$ decays exponentially with time and is therefore zero in the sinusoid steady state. The expression for $\rho(t)$ is

$$\rho(t) = \rho_f \, e^{-(\frac{\sigma}{\varepsilon})t}$$

where ρ_f is the free-charge density at $t = 0$. For example, the time constant $\frac{\sigma}{\varepsilon}$ for copper is 10^{-19} second.

(b) $$\nabla x\ E_z(x,y,t) = -\frac{\partial B_t(x,y,t)}{\partial t}$$ (Faraday's Law)

Here $B_t(x,y,t) = \mu\ H_t(x,y,t)$ and Ohm's Law can be expressed as

$$E_z(x,y,t) = \frac{1}{\sigma}\ J_z(x,y,t)$$

On substituting, one has

$$\frac{1}{\sigma}\ \nabla x\ J_z(x,y,t) = -\mu\ \frac{\partial H_t(x,y,t)}{\partial t} \qquad \text{D.2}$$

(c) $$\nabla x\ H_t(x,y,t) = J_z(x,y,t) + \frac{\partial D_z(x,y,t)}{\partial t} \qquad \text{D.3}$$

where $D_z(x,y,t) = \varepsilon\ E_z(x,y,t)$

Thus $D_z(x,y,t) = \frac{\varepsilon}{\sigma}\ J_z(x,y,t)$

and equation D.3 becomes

$$\nabla x\ H_t(x,y,t) = J_z(x,y,t) + \frac{\varepsilon}{\sigma}\ \frac{\partial J_z(x,y,t)}{\partial t} \qquad \text{D.4}$$

If the curl of equation D.2 is taken there results

$$\nabla x\ \left[\frac{1}{\sigma}\ \nabla x\ J_z(x,y,t)\right] = \nabla x\ \left[-\mu\ \frac{\partial H_t(x,y,t)}{\partial t}\right]$$

or

$$\frac{1}{\sigma}\ \nabla x\ [\nabla x\ J_z(x,y,t)] = -\mu\ \frac{\partial}{\partial t}\ [\nabla x\ H_t(x,y,t)] \qquad \text{D.5}$$

From vector calculus, one has the identity

$$\nabla x\ [\nabla x\ J_z(x,y,t)] = \nabla[\nabla \cdot J_z(x,y,t)] - \nabla^2 J_z(x,y,t)$$

When equation D.4 is substituted into equation D.5 and the

identity used, one obtains

$$\frac{1}{\sigma}\left[\nabla(\nabla\cdot J_z(x,y,t)\ ) - \nabla^2 J_z(x,y,t) = -\mu\frac{\partial}{\partial t}\left[J_z(x,y,t) + \frac{\varepsilon}{\sigma}\frac{\partial J_z(x,y,t)}{\partial t}\right]\right. \qquad \text{D.6}$$

With Ohm's law and equation D.1 one has

$$\nabla\cdot J_z(x,y,t) = 0$$

Equation D.6 now can be written as

$$\nabla^2 J_z(x,y,t) - \mu\sigma\frac{\partial J_z(x,y,t)}{\partial t} - \mu\varepsilon\frac{\partial^2 J_z(x,y,t)}{\partial t^2} = 0 \qquad \text{D.7}$$

Since sinusoid excitation has been assumed, the current density in its most general form can be expressed as

$$J_z(x,y,t) = J_z(x,y,\omega)\, e^{j\omega t} \qquad \text{D.8}$$

where

$$J_z(x,y,\omega) = |J_z(x,y,\omega)|e^{j\alpha(x,y,\omega)}$$

Here $|J_z(x,y,\omega)|$ and $\alpha(x,y,\omega)$ describe the amplitude and phase distribution of the conductor current density. The surface current density is

$$J_s(t) = |J_s(\omega)|e^{j\omega t}$$

and represents a zero phase reference with respect to $\alpha(x,y,\omega)$.

When equation D.8 is substituted into D.7 one has

$$\nabla^2 J_z(x,y,\omega) - j\omega\mu\sigma\, J_z(x,y,\omega) + \omega^2\, \mu\varepsilon\, J_z(x,y,\omega) = 0$$

For the case of a good conductor even at very high radio frequencies, the second coefficient of $J_z(x,y,\omega)$ is extremely small with respect to the absolute value of the first. The resultant equation

$$\nabla^2 J_z(x,y,\omega) - j\,\omega\,\mu_o\mu_r\, J_z(x,y,\omega) = 0 \qquad \text{D.9}$$

describes the two-dimensional current density as a function of frequency. This is the governing equation for the skin effect phenomenon in a good conductor.[10,11,12]

APPENDIX E

Current Density Distribution in a Circular Conductor

Consider a long homogeneous isotropic conductor of circular cross-section lying along the z axis. The conductor is sinusoidally excited at an angular frequency ω .

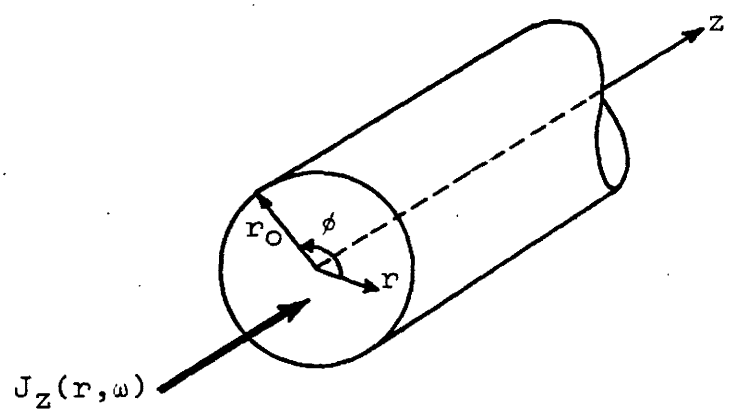

From Faraday's law written in the sinusoid steady-state one has

$$\nabla x\ E_z(r,\omega) = -j\omega\ B_\phi(r,\omega) \qquad \text{E.1}$$

Taking the curl of the above equation one has

$$\nabla x\ [\nabla x\ E_z(r,\omega)] = \nabla[\nabla \cdot E_z(r,\omega)] - \nabla^2 E_z(r,\omega) = -j\omega\mu\ \nabla x\ H_\phi(r,\omega) \qquad \text{E.2}$$

since $\qquad B_\phi(r,\omega) = \mu\ H_\phi(r,\omega)$

In a good conductor even at high radio frequencies the following relations apply:-

(i) $E_z(r,\omega) = \frac{1}{\sigma} J_z(r,\omega)$ E.3

(Ohm's law)

(ii) $\nabla \cdot E_z(r,\omega) = 0$ E.4

(zero free charges)

(iii) $\nabla \times H_\phi(r,\omega) = J_z(r,\omega)$ E.5

(displacement current is negligible compared to the conduction current).

Substitution of E.3, E.4, and E.5 in E.2 gives

$$\nabla^2 J_z(r,\omega) - j\omega\mu\sigma\, J_z(r,\omega) = 0$$

In cylindrical co-ordinates r, ϕ, and z, the above equation becomes

$$\frac{d^2 J_z(r,\omega)}{dr^2} + \frac{1}{r}\frac{dJ_z(r,\omega)}{dr} + \tau^2 J_z(r,\omega) = 0 \qquad \text{E.6}$$

where

$$\tau = j^{-\frac{1}{2}} (\omega\mu\sigma)^{\frac{1}{2}} \qquad \text{E.7}$$

The general solution to this differential equation is given by

$$J_z(r,\omega) = A J_o(\tau r) + B Y_o(\tau r)$$

where $J_o(\tau r)$ and $Y_o(\tau r)$ are Bessel functions of the first

and second kinds with complex arguments.

One must have $r = 0$ in the solution of $J_z(r,\omega)$. As $r \to 0$, $Y_o(\tau r) \to \infty$ and to prevent infinite current density on the axis of the conductor one concludes that $B = 0$. When $r = r_o$, $J_z(r,\omega) = J_s$ where J_s is the surface current density.

Therefore

$$A = \frac{J_s}{J_o(\tau r_o)}$$

Thus, the current density distribution is given by

$$J_z(r,\omega) = J_s \frac{J_o(\tau r)}{J_o(\tau r_o)} \qquad \text{E.8}$$

REFERENCES

1. Vitkovitch, D., Field Analysis: Experimental and Computational Methods, Van Nostrand, London, 1966.

2. Peierls, R.E., "Use of Electrolytic Tank for Magnetic Problems", NATURE, Vol.158, pp.831-832, 1946.

3. Simmons, W.R., "Analogue for Solution of Heat Conduction Problems", CHEMICAL ENGINEERING PROGRESS SYMPOSIUM, Vol.52, p.123, 1956.

4. Surowiak, S., "The Solution of Distributed Field Problems with the Conducting Paper Analogue", AEI ENGINEERING, pp.127-130, May/June, 1965.

5. Delhaye, J., "Conducting Paper Analogue for the Study of Leakage Fields in a Transformer", R.G.E., Vol. 78, No.2, pp.167-176, Feb. 1969.

6. Gilbert, E.O. and Gilbert, E.G., "A Capacitively-Coupled Field Mapper", I.E.E.E. TRANSACTIONS, Vol.72, Part 1, pp.345-349, 1953.

7. Lourie, S.I., "Modelling of Magnetic Fields of Transformers", ELEKTROTECHNIKA, pp.54-57, July 1965.

8. Lourie, S.I., "Mathematical Modelling of Magnetic Leakage Fields of Transformers and Reactors on Electro-Conducting Paper", ELEKTRITCHESTVO, pp.80-86, October, 1965.

9. Birke, P.V. and Palmer, S. "A Capacitively-Coupled Magnetic Flux Mapper", I.E.E.E. Winter Power Meeting, New York, January 1970.

10. Ramo, S., Whinnery, J.R., and Van Duzer, T., Fields and Waves in Communication Electronics, J. Wiley & Sons Inc., New York, 1967.

11. Haus, H.A. and Penhune, J.P., Case Studies in Electromagnetism, J. Wiley and Sons Inc., New York, 1960.

12. Moon, P. and Spencer, D.E., Foundations of Electrodynamics, Van Nostrand, Princeton, N.J., 1960.

13. Khera, R., "Another Realization of an All-Pass Transfer Function Using an Operational Amplifier", I.E.E.E. PROCEEDINGS, Vol.57, No.7, pp.1337-1338, July, 1969.

14. Jahnke-Emde-Lösch, Tables of Higher Functions, McGraw-Hill Book Co.Inc., New York, 1960.